

X-SAM: From Segment Anything to Any Segmentation

Hao Wang^{1,2}, Limeng Qiao³, Zequn Jie³, Zhijian Huang¹, Chengjian Feng³,
Qingfang Zheng², Lin Ma³, Xiangyuan Lan^{2*}, Xiaodan Liang^{1*}

¹Sun Yat-sen University

²Peng Cheng Laboratory

³Meituan Inc.

{wanghao9610, xdliang328}@gmail.com, lanxy@pcl.ac.cn

Abstract

Large Language Models (LLMs) demonstrate strong capabilities in broad knowledge representation, yet they are inherently deficient in pixel-level perceptual understanding. Although the Segment Anything Model (SAM) represents a significant advancement in visual-prompt-driven image segmentation, it exhibits notable limitations in multi-mask prediction and category-specific segmentation tasks, and it cannot integrate all segmentation tasks within a unified model architecture. To address these limitations, we present X-SAM, a streamlined Multimodal Large Language Model (MLLM) framework that extends the segmentation paradigm from *segment anything* to *any segmentation*. Specifically, we introduce a novel unified framework that enables more advanced pixel-level perceptual comprehension for MLLMs. Furthermore, we propose a new segmentation task, termed Visual Grounded (VGD) segmentation, which segments all instance objects with interactive visual prompts and empowers MLLMs with visual grounded, pixel-wise interpretative capabilities. To enable effective training on diverse data sources, we present a unified training strategy that supports co-training across multiple datasets. Experimental results demonstrate that X-SAM achieves state-of-the-art performance on a wide range of image segmentation benchmarks, highlighting its efficiency for multimodal, pixel-level visual understanding. Code is available at <https://github.com/wanghao9610/X-SAM>.

Introduction

Multi-modal Large Language Models (MLLMs) have exhibited substantial advancements alongside the rapid development of Large Language Models (LLMs) (Bai et al. 2023; Touvron et al. 2023) and multi-modal pre-training methods (Radford et al. 2021; Jia et al. 2021). These models have shown remarkable effectiveness in a wide range of applications, including image captioning (Xu et al. 2015), VQA (Antol et al. 2015), and visual editing (Chen et al. 2018). However, current MLLMs lack the capability to generate dense pixel-level outputs for precise spatial understanding. This limitation poses a considerable challenge in directly addressing tasks that require pixel-level comprehen-

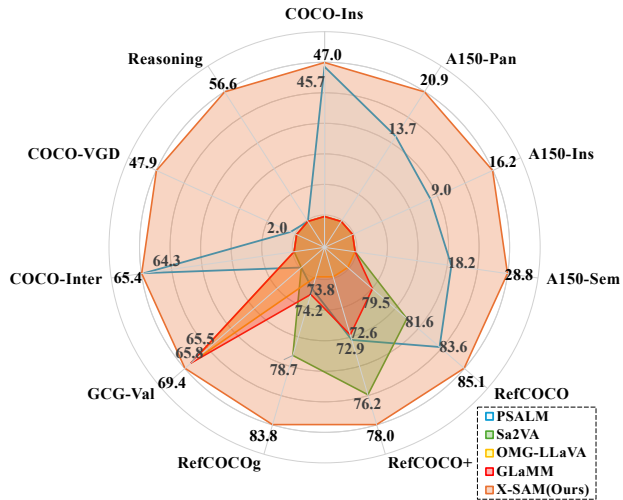


Figure 1: Illustration of Performance of X-SAM on Image Segmentation Benchmarks. X-SAM consistently surpasses existing Multimodal Large Language Models (MLLMs) across all evaluated segmentation benchmarks.

sion of visual data, such as image segmentation, which is the most critical task in the field of computer vision.

The Segment Anything Model (SAM) represents a foundational segmentation model that demonstrates exceptional efficacy in generating dense segmentation masks and has inspired the development of various segmentation tasks, such as high-quality segmentation (Ke et al. 2023), matching anything (Li et al. 2024c), and tracking anything (Rajić et al. 2025). Nevertheless, SAM’s architecture is fundamentally constrained by its dependency on visual prompts, which significantly limits its direct applicability to a wide range of image segmentation tasks, including generic (semantic, instance, panoptic) segmentation, referring segmentation, and open-vocabulary (OV) segmentation, among others. Achieving a unified framework capable of addressing various image segmentation tasks remains a challenging problem.

In this work, we introduce X-SAM, an innovative framework that unifies diverse image segmentation tasks, expanding the segmentation paradigm from *segment anything* to *any segmentation*. To accomplish this objective, our approach addresses three critical technical challenges: (1) *Task*

*Corresponding author.

Copyright © 2026, Association for the Advancement of Artificial Intelligence (www.aaai.org). All rights reserved.

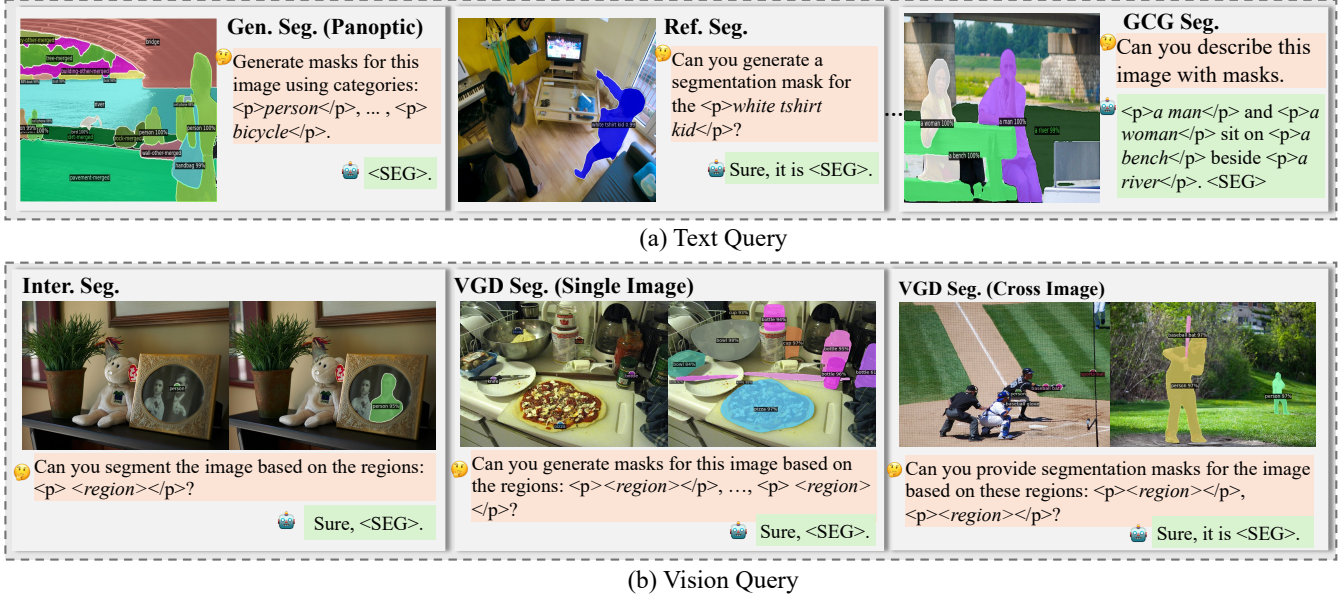


Figure 2: Illustration of the capabilities of X-SAM. (a). Text query tasks: Generic (Gen.), Referring(Ref.), Reasoning(Rea.), and Grounded Conversation Generation(GCG) segmentation, *etc..* (b). Vision query tasks: Interactive(Inter.) and Visual GrounDed (VGD) segmentation for single and cross-image.

formulation: Transforming SAM into a versatile segmentation architecture with cross-task applicability. (2) *Modality enhancement*: Augmenting LLMs with multimodal input processing capabilities. (3) *Unified framework*: Developing a cohesive approach to effectively facilitate comprehensive segmentation applications across diverse domains.

First, we develop a unified segmentation MLLM architecture that incorporates a unified mask decoder capable of generating segmentation masks suitable for generalized image segmentation tasks. Second, we expand the multimodal capabilities of MLLMs to process not only textual queries but also visual queries. Specifically, we introduce a novel task termed Visual GrounDed (VGD) segmentation, which segments all instance objects with interactive visual prompts in an image. This task introduces visual guide modalities into large language models (LLMs). Moreover, we propose a unified input format and training methodology that reformulates segmentation tasks within a unified framework, thus optimizing the adaptation of MLLMs to diverse image segmentation tasks.

As shown in Figure 2 and Table 1, we present the comprehensive capabilities of X-SAM and compare them with those of other methods. Our proposed framework exhibits capabilities in processing text query-based tasks, such as generic segmentation and referring segmentation, while simultaneously accommodating vision query-based tasks such as interactive segmentation (Zhang et al. 2024c) and our novel VGD segmentation, which functions effectively in both single-image and cross-image contexts. Furthermore, X-SAM leverages the reasoning and generative capacities of LLMs, thereby enabling advanced reasoning segmentation and Grounded Conversation Generation (GCG) (Rasheed et al. 2024) segmentation.

X-SAM undergoes co-training with a diverse range of datasets. We perform a comprehensive evaluation on more than twenty segmentation datasets across seven distinct image segmentation tasks, even including the image conversion task. X-SAM achieves the state-of-the-art performance across all image segmentation benchmarks, and establishes a robust new baseline for unified pixel-level image understanding, as illustrated in Figure 1. In summary, our contributions are as follows:

- We introduce X-SAM, a novel unified framework that extends the segmentation paradigm from *segment anything* to *any segmentation*. Our approach formulates diverse image segmentation tasks into a standardized segmentation format.
- We propose a new image segmentation benchmark, Visual GrounDed (VGD) segmentation, which provides visual grounded prompts for MLLMs to segment instance objects in images. The benchmark introduces user-friendly inputs to ground the segmentation objects and guide the MLLMs to output the segmentation masks.
- We present a unified multi-stage training strategy to co-train X-SAM with a diverse range of datasets, and conduct extensive evaluations on more than twenty image segmentation benchmarks, achieving state-of-the-art performance on all of them. This establishes a new strong baseline for unified pixel-level perceptual understanding in MLLMs.

Related Work

Multi-modal Large Language Model. Multi-modal learning has evolved from early models focused on task-specific fusion and feature extraction (Li et al. 2022b), to leveraging

Method	Text Query						Vision Query		
	Gen. Seg.	OV Seg.	Ref. Seg.	Rea. Seg.	GCG Seg.	Inter. Seg.	VGD Seg.		
SAM(Kirillov et al. 2023a)							✓		
Mask2Former(Cheng et al. 2022a)	✓								
ODISE(Xu et al. 2023)	✓		✓						
UNINEXT(Yan et al. 2023)	✓			✓			✓		
SEEM(Zou et al. 2023b)	✓		✓	✓			✓		
OMG-Seg(Li et al. 2024d)	✓		✓				✓		
LISA(Lai et al. 2024)				✓	✓				
GLaMM(Rasheed et al. 2024)				✓		✓			
PixelLM(Zhang et al. 2024c)				✓					
OMG-LLaVA(Zhang et al. 2024a)	✓			✓		✓			
Sa2VA(Yuan et al. 2025)				✓	✓	✓			
PSALM(Zhang et al. 2024c)	✓	✓	✓	✓			✓		
X-SAM (Ours)	✓	✓	✓	✓	✓	✓	✓	✓	

Table 1: Comparison of Capability. We compare different methods on both segmentation-specific (Gray) and MLLM-based.

large language models (Brown et al. 2020; Touvron et al. 2023) for generalized, instruction-tuned multi-task benchmarks (Liu et al. 2024b; Hudson et al. 2019). LLaVA (Liu et al. 2023a, 2024a) introduced visual feature tokenization, inspiring advances in visual representation (Yuan et al. 2024b), specialized vision extensions (Lai et al. 2024; Lin et al. 2023), and language-guided segmentation (Li et al. 2024d; Zhang et al. 2024b). However, most progress remains task-specific. To our knowledge, we are the first to successfully implement a comprehensive approach, opening new directions for image segmentation.

Multi-modal Grounded Segmentation. Recent works (Pan et al. 2024; Wang et al. 2023) explore visual initiation methods in vision, including learnable tokens (Zhou et al. 2022a), mask-visual-modeling (Fang et al. 2023), and visual prompting encoders (Yuan et al. 2024a). SAM (Kirillov et al. 2023b) and its extensions (Xu et al. 2024) introduce visual grounding signals to segmentation models, greatly improving performance. Interactive segmentation (Li et al. 2024d) further enhances user-guided segmentation for MLLMs. However, existing methods cannot freely treat grounded input as textual input for segmentation. To address this, we propose Visual GrounDed (VGD) segmentation, enabling more diverse multi-modal grounded segmentation.

Unified Segmentation Model. Vision transformers (Dosovitskiy et al. 2020) have advanced universal segmentation, with recent works (Xu et al. 2024; Cheng et al. 2022b) developing end-to-end mask classification frameworks that outperform earlier models (Zhou et al. 2022b; Wang et al. 2021a) across various applications. Research has expanded to open-world and open-vocabulary segmentation (Yuan et al. 2024a; Qi et al. 2022a,b), as well as unified architectures for multiple tasks (Athar et al. 2023; Jain et al. 2023; Li et al. 2024d). However, most methods focus solely on visual segmentation and lack interactive textual and visual prompts found in MLLMs. To address this, we combine SAM with MLLMs, extending SAM from *segment anything* to *any segmentation*, and introduce a unified framework adaptable to all image segmentation tasks, establishing a strong baseline.

Method

To achieve unified image segmentation, we present X-SAM, a novel multi-modal segmentation MLLM. We design a versatile input format and a unified framework to integrate diverse segmentation tasks into a single model. Additionally, we introduce an innovative training strategy that enables SAM to handle any segmentation task. The following sections detail our methodology.

Formulation

The development of a unified segmentation model is fraught with challenges stemming from the diverse nature of segmentation tasks and the variability in input format. To address these issues, we introduce a versatile input format tailored to support a wide range of image segmentation tasks, laying the groundwork for the unified framework of X-SAM. We delineate the input format into two primary categories: text query input and vision query input. The text query input consists exclusively of linguistic prompts derived from user requests, the vision query input integrates both linguistic prompts and visual prompts provided by the user.

Text Query Input. The majority of existing image segmentation tasks can be conceptualized as text query inputs, including generic segmentation (Kirillov et al. 2019), referring segmentation, open-vocabulary (OV) segmentation (Li et al. 2022a), GCG segmentation (Rasheed et al. 2024), and reasoning segmentation (Lai et al. 2024). A text query input encapsulates the user’s request along with the specific category or object to be segmented, which may be embedded within the user’s prompt or generated by a large language model (LLM). To facilitate the GCG segmentation task, inspired by GLaMM (Rasheed et al. 2024), we incorporate two special phrase tokens, $\langle p \rangle$ and $\langle /p \rangle$, into the tokenizer to denote the beginning and end of a phrase, respectively. For each category in generic segmentation and GCG segmentation, phrase in referring segmentation, or sentence in reasoning segmentation, the format is standardized as

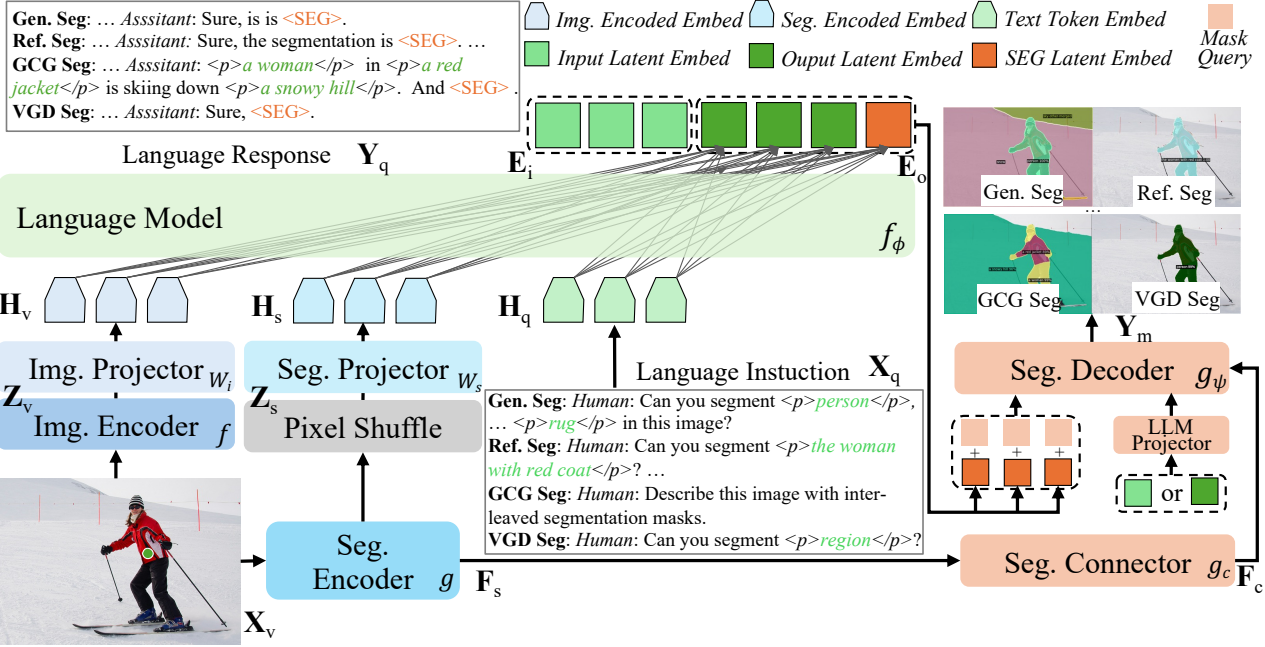


Figure 3: The Overview of X-SAM. X-SAM comprises dual encoders, dual projectors, a language model, a segmentation connector, and a segmentation decoder. The dual encoders process the image and project features to match text embedding dimensions, which are then input to the language model with tokenized text for instruction-guided understanding. The SAM features are connected to the segmentation decoder, which uses the LLM’s `<SEG>` token to generate segmentation masks.

“`<p>category/phrase/sentence</p>`”. Specifically, the `<p>` and `</p>` tokens are not only encoded in the input tokens but also generated in the output tokens, ensuring consistency across different tasks. Additionally, for the output, we introduce a special token `<SEG>` into the tokenizer to signify the segmentation result, following the approach in (Lai et al. 2024).

Vision Query Input. Beyond text query inputs, some tasks necessitate vision query inputs, such as interactive segmentation (Zhang et al. 2024c) and the Visual GrounDed segmentation proposed in this work. In contrast to text query inputs, vision query inputs incorporate a visual prompt from the user, which may take the form of points, scribbles, boxes, or masks. To denote the visual prompt, we employ a dedicated token, `<region>`, within the input format. Analogous to the text query input, the visual prompt is formatted as “`<p><region></p>`” and the segmentation output is similarly indicated by the `<SEG>` token. The `<region>` token serves as a placeholder for the visual prompt and will be replaced by the region feature extracted from the segmentation encoder.

Unified Formulation. The latent language embeddings between the `<p>` and `</p>` tokens are used as the condition embeddings for the segmentation decoder to compute the classification scores. Based on this formulation, we achieve a unified framework for all image segmentation tasks. Given an input image $\mathbf{X}_v \in \mathbb{R}^{H \times W \times 3}$ and a language instruction $\mathbf{X}_q \in \mathbb{R}^{P \times 1}$, the model takes the image and language instruction as inputs and outputs a language response $\mathbf{Y}_q \in \mathbb{R}^{L \times 1}$ and a segmentation mask $\mathbf{Y}_m \in \mathbb{R}^{H \times W}$. Here,

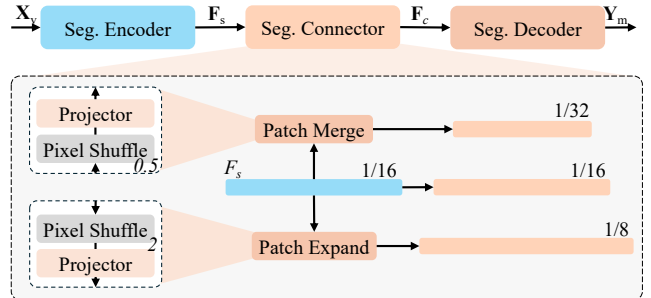


Figure 4: The Architecture of Segmentation Connector.

P is the length of the input text tokens, and L is the total length of the input and output text tokens. H and W denote the height and width of the image, respectively. Detailed input format examples can be found in Figure 2 (a) and (b).

Architecture

In this section, we propose X-SAM, a unified segmentation MLLM for any segmentation. As shown in Figure 3, it includes dual encoders, dual projectors, an LLM, a segmentation connector, and a segmentation decoder.

Dual Encoders. There are two encoders in X-SAM, an image encoder and a segmentation encoder. The image encoder f is used to extract the global image feature $\mathbf{Z}_v = f(\mathbf{X}_v)$, while the segmentation encoder g extracts the fine-grained image feature $\mathbf{Z}_s = g(\mathbf{X}_v)$. The feature from the image encoder is global and benefits image understanding tasks,

Method	Gen. Seg. Pan. / Ins. / Sem.	OV Seg. Pan. / Ins. / Sem.	Ref. Seg. RefCOCO / + / g	Rea. Seg. Val / Test	GCG Seg. Val / Test	Inter. Seg. Point / Box	VDG Seg. Point / Box
SAM-L(Kirillov et al. 2023a)	\times	\times	\times	\times	\times	51.8 / 76.6	12.8 / 31.7
Mask2Former-L(Cheng et al. 2022a)	57.8 / 48.6 / 67.4	\times	\times	\times	\times	\times	\times
SEEM-B(Zou et al. 2023b)	56.1 / 46.4 / 66.3	\times	- / - / 65.6	\times	\times	47.8 / 44.9	\times
ODISE(Xu et al. 2023)	55.4 / 46.0 / 65.2	22.6 / 14.4 / 29.9	\times	\times	\times	\times	\times
OMG-Seg(Li et al. 2024d)	53.8 / - / -	\times	\times	\times	\times	-	\times
LISA-7B(Lai et al. 2024)	\times	\times	74.9 / 65.1 / 67.9	<u>52.9 / 47.3</u>	\times	\times	\times
GLaMM(Rasheed et al. 2024)	\times	\times	79.5 / 72.6 / 74.2	\times	<u>65.8 / 64.6</u>	\times	\times
PixelLM-7B(Ren et al. 2024)	\times	\times	73.0 / 66.3 / 69.3	\times	\times	\times	\times
OMG-LLaVA-7B(Zhang et al. 2024a)	53.8 / - / -	\times	78.0 / 69.1 / 72.9	\times	<u>65.5 / 64.7</u>	\times	\times
Sa2VA-8B(Yuan et al. 2025)	\times	\times	81.6 / <u>76.2 / 78.7</u>	- / -	- / -	\times	\times
PSALM(Zhang et al. 2024c)	55.9 / 45.7 / 66.6	<u>13.7 / 9.0 / 18.2</u>	83.6 / 72.9 / 73.8	\times	\times	64.3 / 67.3	2.0 / 3.7
X-SAM (Ours)	54.7 / 47.0 / 66.5	20.9 / 16.2 / 28.8	85.1 / 78.0 / 83.8	56.6 / 57.8	69.4 / 69.0	65.4 / 70.0	47.9 / 49.5

Table 2: Comprehensive Performance Comparison. We compare X-SAM to segmentation-specific models (Gray) and MLLMs. “ \times ” denotes unsupported tasks. “-” indicates unreported results. X-SAM achieves state-of-the-art performance across all segmentation tasks with a single model. Best results are in **bold**, second-best are underlined.

whereas the feature from the segmentation encoder is fine-grained and benefits image segmentation tasks. We adopt SigLIP2-so400m (Tschannen et al. 2025) as the image encoder and SAM-L (Ke et al. 2023) as the segmentation encoder.

Dual Projectors. To enhance the LLM’s understanding of the image, we concatenate the features from the image encoder and the segmentation encoder before passing them to the LLM. Specifically, the feature from the segmentation encoder is too large to be processed directly by the LLM, so we utilize a pixel-shuffle operation to reduce its spatial size. We then project the reduced feature into the language embedding space \mathbf{H}_q via an MLP projector W_s . For the feature from the image encoder, we directly project it into the language embedding space via an MLP projector W_i , such that $\mathbf{H}_v = W_i \cdot \mathbf{Z}_v$ and $\mathbf{H}_s = W_s \cdot \mathbf{Z}_s$. We then concatenate the features from dual projectors and the language embeddings, and input them into the LLM f_ϕ .

Segmentation Connector. For image segmentation tasks, fine-grained multi-scale features are crucial for the segmentation decoder to accurately predict segmentation masks. The output of the segmentation encoder in SAM is single-scale (1/16) with reduced spatial resolution. To obtain multi-scale features, we design a segmentation connector g_c , to bridge the segmentation encoder and decoder. As shown in Figure 4, we perform patch-merge using a pixel-shuffle (Chen et al. 2024) with a scale of 0.5 to reduce the spatial size of the last feature in the encoder to a smaller scale (1/32). We also perform patch-expand with a pixel-shuffle of scale 2.0 to increase the spatial size of the last feature to a larger scale (1/8), resulting in multi-scale features for the segmentation decoder.

Segmentation Decoder. The Segment Anything Model (SAM) can segment a single object based on input text or visual prompts, but it fails to segment all objects in a single inference. To segment all objects at once, we replace its original segmentation decoder with a new decoder, following the approach in (Cheng et al. 2022a; VS et al. 2024). The segmentation decoder g_ψ predicts masks and their category probabilities from either the input latent embedding \mathbf{E}_i

or the output latent embedding \mathbf{E}_o , multi-scale segmentation features \mathbf{F}_c , and a set of mask query tokens plus the $\langle \text{SEG} \rangle$ token embedding, which bridges the LLM output with the segmentation decoder. Notably, we introduce a latent background embedding to represent the “ignore” category for all tasks, thereby unifying all image segmentation tasks with one model.

Training

To improve the performance on diverse image segmentation tasks, we propose a novel multi-stage training strategy. The training strategy consists of three stages: segmentor fine-tuning, alignment pre-training, and mixed fine-tuning.

Stage 1: Segmentor Fine-tuning. As the segmentation decoder is redesigned, we need to train the segmentor to adapt to segment all objects in a single forward pass. We follow the training pipeline in (Cheng et al. 2022a), which trains the model on the popular COCO-Panoptic (Kirillov et al. 2019) dataset. To enable faster convergence during training, we unfreeze all the parameters in the segmentor while training the segmentation encoder with a lower learning rate. The training objective, \mathcal{L}_{seg} , is the same as in (Cheng et al. 2022a), and is defined as the sum of the classification loss \mathcal{L}_{cls} , the mask loss $\mathcal{L}_{\text{mask}}$, and the dice loss $\mathcal{L}_{\text{dice}}$:

$$\mathcal{L}_{\text{seg}} = \mathcal{L}_{\text{cls}} + \mathcal{L}_{\text{mask}} + \mathcal{L}_{\text{dice}} \quad (1)$$

Stage 2: Alignment Pre-training. To align the language embeddings and visual embeddings, we perform alignment pre-training on the LLaVA-558K dataset, following (Liu et al. 2023b). We keep the dual encoders and the LLM parameters frozen, and only train the dual projectors. In this way, the image embeddings and segmentation embeddings can be aligned with the pre-trained LLM word embeddings. The training objective for alignment pre-training is an autoregressive loss $\mathcal{L}_{\text{regressive}}$:

$$\mathcal{L}_{\text{regressive}} = - \sum_{i=1}^N \log p_\theta \left(\mathcal{Y}_q^{[P+i]} | \mathcal{Y}_q^{[:i-1]}, \mathcal{X}_q^{[:i-1]} \right), \quad (2)$$

where \mathcal{X}_q is the input sequence $\mathcal{X}_q = [x_1, x_2, \dots, x_p] \in \mathbb{R}^{P \times D}$, \mathcal{Y}_q is the output sequence $\mathcal{Y}_q = [y_1, y_2, \dots, y_l] \in$

Method	(M)LLM	RefCOCO			RefCOCO+			RefCOCOg	
		val	testA	testB	val	testA	testB	val	test
SEEM-L (Zou et al. 2023b)	-	-	-	-	-	-	-	65.6	-
UNINEXT-L (Yan et al. 2023)	-	80.3	82.6	77.8	70.0	74.9	62.6	73.4	73.7
UNINEXT-H (Yan et al. 2023)	-	82.2	83.4	81.3	72.5	76.4	66.2	74.7	76.4
GLaMM (Rasheed et al. 2024)	Vicuna-7B	79.5	83.2	76.9	72.6	78.7	64.6	74.2	74.9
OMG-LLaVA (Zhang et al. 2024a)	InternLM-7B	77.2	79.8	74.1	68.7	73.0	61.6	71.7	71.9
Sa2VA(Yuan et al. 2025)	InternVL2-8B	81.6	-	-	76.2	-	-	78.7	-
PSALM (Zhang et al. 2024c)	Phi-1.5-1.3B	83.6	84.7	81.6	72.9	75.5	70.1	73.8	74.4
HyperSeg (Wei et al. 2024b)	Miphia-3B	84.8	85.7	83.4	79.0	83.5	75.2	79.4	78.9
X-SAM (Ours)	Phi-3-3.8B	85.1	87.1	83.4	78.0	81.0	74.4	83.8	83.9

Table 3: Comparison of Referring Segmentation. We evaluate methods on referring segmentation benchmarks by (M)LLMs.

$\mathbb{R}^{L \times D}$, where $L = P + N$ represents the length of output sequence, D represents the hidden size of LLM. θ is a trainable parameter in LLM, and we only calculate the loss for the generated text.

Stage 3: Mixed Fine-tuning. X-SAM is co-trained on multiple datasets across diverse tasks in an end-to-end manner. For the image conversation task, we adopt the auto-regressive loss $\mathcal{L}_{\text{regressive}}$ as is common in MLLM training. For the segmentation tasks, we not only use the segmentation loss as in segmentor training, but also add the auto-regressive loss to the training objective. Benefiting from the unified formulation and simple training objective, end-to-end mixed fine-tuning across diverse tasks can be performed within a unified framework. The training objective for mixed fine-tuning can be formulated as:

$$\mathcal{L}_{\text{total}} = \begin{cases} \mathcal{L}_{\text{regressive}}, & \text{conversation} \\ \mathcal{L}_{\text{regressive}} + \mathcal{L}_{\text{seg}}, & \text{segmentation} \end{cases} \quad (3)$$

Experiments

Experiment Settings

Datasets and Tasks. For segmentor fine-tuning, we train on the COCO-Panoptic (Kirillov et al. 2019) dataset. For alignment pre-training, we utilize the LLaVA-558K (Liu et al. 2023b) dataset. For end-to-end mixed fine-tuning, we incorporate one image conversation dataset and five types of image segmentation datasets into the training process. To balance the training data across these diverse datasets, we set the training epoch to 1 and adjust the resampling rates of different datasets using dataset balance resampling. After training, X-SAM is capable of performing a variety of tasks, including Image Conversation, Generic, Referring, Reasoning, GCG, Interactive, and VGD Segmentation. Additionally, X-SAM supports Open-Vocabulary (OV) (OV-semantic, OV-instance, OV-panoptic) segmentation, enabling it to segment all objects defined by the input prompt, even those never seen before. Note that COCO-VGD is our proposed VGD segmentation dataset, which is built on the COCO2017 dataset.

Evaluation Metrics. We conduct extensive experiments to evaluate the performance of X-SAM. For generic segmentation and open-vocabulary segmentation, we use PQ, mIoU,

and mAP as the main metrics for panoptic, semantic, and instance segmentation, respectively. For referring segmentation and reasoning segmentation, we adopt cIoU and gIoU as metrics, following (Zhang et al. 2024c). For GCG segmentation, we use M, C, AP50, and mIoU as metrics, following (Rasheed et al. 2024). For interactive segmentation, we use mIoU and cIoU, also following (Zhang et al. 2024c). For VGD segmentation, we use AP and AP50. For image conversation, we adopt scores from common MLLM benchmarks as the main metrics, following (Liu et al. 2023b).

Implementation Details. We adopt the XTuner (Contributors 2023) codebase for training and evaluation. During segmentor fine-tuning, we train all parameters, set the batch size to 64, and use a learning rate of 1e-5 for the SAM encoder and 1e-4 for the other parameters. The number of training epochs is set to 36. For alignment pre-training, we train only the dual projector parameters, with a batch size of 256, a learning rate of 1e-3, and one training epoch. For end-to-end mixed fine-tuning, we train all parameters, set the batch size to 64, and use a learning rate of 4e-6 for the dual encoders and 4e-5 for the other parameters, with one training epoch. All training is conducted on 16 A100 GPUs. For image conversation evaluation, we use the VLMEvalKit (Duan et al. 2024) codebase to evaluate performance on MLLM benchmarks. For segmentation task evaluation, we follow the settings described in the corresponding papers and repositories.

Main Results

We conduct extensive evaluation on seven segmentation tasks, including Generic, Open-Vocabulary, Referring, Reasoning, GCG, Interactive, and VGD Segmentation.

Overall. In Table 2, we compare X-SAM with current segmentation-specific models and MLLMs. X-SAM demonstrates the most comprehensive capabilities. It achieves performance comparable to state-of-the-art in generic segmentation, and achieves the best performance on other benchmarks, with a single model. X-SAM sets a new state-of-the-art record for image segmentation benchmarks. Detailed results for each task are discussed below.

Referring Segmentation. We evaluate X-SAM on RefCOCO, RefCOCO+, and RefCOCOg, with the results shown in Table 3. X-SAM outperforms PSALM (Zhang et al. 2024c) by 1.5% cIoU, 5.1% cIoU, and 10.0% cIoU

Methods	Val				Test			
	METEOR	CIDEr	AP50	mIoU	METEOR	CIDEr	AP50	mIoU
Kosmos-2(Peng et al. 2023)	16.1	27.6	17.1	55.6	15.8	27.2	17.2	56.8
LISA-7B(Lai et al. 2024)	13.0	33.9	25.2	62.0	12.9	32.2	24.8	61.7
GLaMM-7B [†] (Rasheed et al. 2024)	15.2	43.1	28.9	65.8	14.6	37.9	27.2	64.6
OMG-LLaVA-7B(Zhang et al. 2024a)	14.9	41.2	29.9	65.5	14.5	38.5	28.6	64.7
X-SAM (Ours)	15.4	46.3	33.2	69.4	15.1	42.7	32.9	69.0

Table 4: Comparison of GCG Segmentation. [†] indicates pretraining with the GranD dataset (Rasheed et al. 2024).

Method	Point		Scribble		Box		Mask	
	AP	AP50	AP	AP50	AP	AP50	AP	AP50
PSALM [†] (Zhang et al. 2024c)	2.0	3.3	<u>2.8</u>	<u>4.4</u>	3.7	5.8	<u>2.3</u>	<u>3.3</u>
SAM [†] (Kirillov et al. 2023b)	<u>12.8</u>	<u>22.8</u>	-	-	<u>31.7</u>	<u>50.1</u>	-	-
X-SAM (Ours)	47.9	72.5	48.7	73.4	49.5	74.7	49.7	74.9

Table 5: Comparison of VGD Segmentation. [†] indicates evaluation results following X-SAM setting.

FT	COCO-Pan	A150-OV	RefCOCO	Reason-Val
	PQ	PQ	cloU	gIoU
Specific	55.3	16.4	81.0	48.2
Mixed	54.5(↓ 0.8)	22.4(↑ 6.0)	85.4(↑ 4.4)	57.1(↑ 8.9)

Table 6: Ablation on Fine-Tuning(FT).

Encoder	COCO-Pan	A150-OV	GCG-Val	COCO-VGD
	PQ	PQ	mIoU	AP
ViT -	54.5	16.4	64.8	40.7
ViT Swin [†]	56.2(↑ 1.7)	18.6(↑ 2.2)	62.5(↓ 2.3)	48.6(↑ 7.9)
ViT SAM	54.7(↑ 0.2)	20.9(↑ 4.5)	69.4(↑ 4.6)	47.9(↑ 7.2)

Table 7: Ablation on Dual Encoders. Swin[†] is initialized from Mask2Former (M2F) (Cheng et al. 2022a).

on the validation sets of RefCOCO, RefCOCO+, and RefCOCOg, respectively. Compared to Sa2VA-8B (Yuan et al. 2025), X-SAM achieves better results with a smaller model size. It shows performance improvements of 3.5% cloU, 1.8% cloU, and 5.1% cloU on RefCOCO, RefCOCO+, and RefCOCOg, respectively.

GCG Segmentation. Grounded conversation demands detailed image and pixel-level understanding, requiring MLLMs to link captioned objects to their segmentation masks. As shown in Table 4, X-SAM achieves a significant performance improvement compared to previous methods and obtains the best results on both the Val and Test sets. In terms of image-level understanding, X-SAM outperforms GLaMM (Rasheed et al. 2024) by 0.2% METEOR and 3.2% CIDEr on the Val set, and by 0.5% METEOR and 4.8% CIDEr on the Test set. In terms of pixel-level understanding, X-SAM outperforms OMG-LLaVA (Zhang et al. 2024a) by 3.3% AP and 3.9% mIoU on the Val set, and by 4.3% AP and 4.3% mIoU on the Test set.

VGD Segmentation. Visual grounded segmentation de-

mands vision query understanding, requiring MLLMs to comprehend the visual modality and segment all related instances. Table 5 presents the VGD segmentation results. As VGD segmentation is our newly proposed task, we evaluate PSALM (Zhang et al. 2024c) following X-SAM’s settings. X-SAM outperforms PSALM by 45.9% AP, 45.9% AP, 45.8% AP, and 47.4% AP on Point, Scribble, Box, and Mask visual prompts, respectively.

Ablations

We conduct ablation studies on mixed fine-tuning, dual encoders, multi-stage training, and segmentor architecture, presenting selected benchmark results due to space limitations.

Mixed Fine-tuning. We ablate the impact of mixed fine-tuning on X-SAM’s performance. As shown in Table 6, mixed fine-tuning improves performance on out-of-domain COCO benchmarks, demonstrating X-SAM’s robust segmentation capabilities—for example, a 6.0% PQ increase on A150-OV and an 8.9% gIoU increase on Reason-Val. However, it results in a 0.8% PQ decrease on COCO-Pan due to the challenge of balancing performance in multi-sources training.

Dual Encoders. We ablate the design of the dual encoders in X-SAM. As shown in Table 7, dual encoders with either a SAM or Swin encoder benefit VGD segmentation, achieving 7.2% AP and 7.9% AP on COCO-VGD, respectively. Moreover, dual encoders with a SAM encoder consistently improve performance on GCG-Val and A150-OV, while the Swin encoder, which lacks robust segmentation capabilities, provides only a small improvement on A150-OV and even has a negative impact on GCG-Val.

Multi-stage Training. We ablate the impact of the multi-stage training strategy. As shown in Table 8, the S1 segmentor fine-tuning phase boosts the segmentation capability, producing a notable improvement of 9.3% PQ in COCO-Pan and 1.5% PQ in the A150-OV datasets. Meanwhile, the S2 alignment pre-training phase enhances image understanding

M-Stage	COCO-Pan PQ	A150-OV PQ	GCG-Val mIoU	Conv.-MMB Acc.
S3	45.2	19.4	60.6	67.2
S1, S3	54.5(↑ 9.3)	20.9(↑ 1.5)	65.4(↑ 4.8)	67.4(↑ 0.2)
S1, S2, S3	54.7(↑ 9.5)	20.9(↑ 1.5)	69.4(↑ 8.8)	69.3(↑ 2.1)

Table 8: Ablation on Multi-Stage(M-Stage) Training. S1: Stage 1, S2: Stage 2, S3: Stage 3, Conv.: conversation.

Conn.	Decoder	M-Scale	PQ	AP	mIoU
-	SAM	✗	40.9	26.3	49.5
MLP	M2F	✗	50.1(↑ 9.2)	38.9(↑ 12.6)	60.2(↑ 10.7)
Con.	M2F	✗	50.3(↑ 9.4)	39.1(↑ 12.8)	60.6(↑ 11.1)
Con.	M2F	✓	51.6(↑ 10.7)	41.5(↑ 15.2)	61.6(↑ 12.1)

Table 9: Ablation on Segmentor Architecture. Conn.: connector, M-Scale: multi-scale, Con.: convolution, M2F: Mask2Former.

capabilities, contributing an additional 2.1% Accuracy on Conv.-MMB. By integrating these stages, X-SAM demonstrates robust advances in image segmentation and comprehension, establishing its effectiveness in addressing complex visual tasks.

Segmentor Architecture. We ablate the impact of segmentor architecture by performing segmentor fine-tuning for 12 epochs. As shown in Table 9, M2F decoder brings a large improvement with 9.2% PQ as the effective design of M2F. The convolution connector performs better than the MLP connector, as the convolution spatial-awareness benefits segmentation, and multi-scale further improves the performance(10.7% PQ) with more diverse scale features.

Conclusion

In this work, we propose X-SAM, a unified segmentation MLLM that extends the segmentation paradigm from *segment anything* to *any segmentation*, integrating all image segmentation tasks into a single model. Our method can process various multimodal inputs in MLLMs, including both text and visual queries. Moreover, to equip MLLMs with visual grounded perception capabilities, we introduce a new segmentation task, Visual Grounded (VGD) segmentation, further extending the capabilities of the unified segmentation model. We conduct extensive experiments across all image segmentation tasks, and X-SAM achieves state-of-the-art performance on each task with a single model.

Acknowledgments

This work is supported by National Key Research and Development Program of China (2024YFE0203100), Scientific Research Innovation Capability Support Project for Young Faculty (No.ZYQXQNJSKYCXNLZCXM-I28), National Natural Science Foundation of China (NSFC) under Grants No.62476293, General Embodied AI Center of Sun Yat-sen University, National Natural Science Foundation of China (62402252) and (62536003) Guangdong High-Level Talent Programme (2024TQ08X283).

References

Abdin, M.; Aneja, J.; Awadalla, H.; Awadallah, A.; Awan, A. A.; Bach, N.; Bahree, A.; Bakhtiari, A.; Bao, J.; Behl, H.; et al. 2024. Phi-3 technical report: A highly capable language model locally on your phone. *arXiv preprint arXiv:2404.14219*.

Antol, S.; Agrawal, A.; Lu, J.; Mitchell, M.; Batra, D.; Zitnick, C. L.; and Parikh, D. 2015. Vqa: Visual question answering. In *Proceedings of the IEEE international conference on computer vision*, 2425–2433.

Athar, A.; Hermans, A.; Luiten, J.; Ramanan, D.; and Leibe, B. 2023. Tarvis: A unified approach for target-based video segmentation. In *Proceedings of the IEEE/CVF Conference on Computer Vision and Pattern Recognition*, 18738–18748.

Bai, J.; Bai, S.; Chu, Y.; Cui, Z.; Dang, K.; Deng, X.; Fan, Y.; Ge, W.; Han, Y.; Huang, F.; et al. 2023. Qwen technical report. *arXiv preprint arXiv:2309.16609*.

Brown, T.; Mann, B.; Ryder, N.; Subbiah, M.; Kaplan, J. D.; Dhariwal, P.; Neelakantan, A.; Shyam, P.; Sastry, G.; Askell, A.; et al. 2020. Language models are few-shot learners. *Advances in neural information processing systems*, 33: 1877–1901.

Chen, J.; Shen, Y.; Gao, J.; Liu, J.; and Liu, X. 2018. Language-based image editing with recurrent attentive models. In *Proceedings of the IEEE conference on computer vision and pattern recognition*, 8721–8729.

Chen, Z.; Wang, W.; Tian, H.; Ye, S.; Gao, Z.; Cui, E.; Tong, W.; Hu, K.; Luo, J.; Ma, Z.; et al. 2024. How far are we to gpt-4v? closing the gap to commercial multimodal models with open-source suites. *Science China Information Sciences*, 67(12): 220101.

Cheng, B.; Misra, I.; Schwing, A. G.; Kirillov, A.; and Girdhar, R. 2022a. Masked-attention mask transformer for universal image segmentation. In *Proceedings of the IEEE/CVF conference on computer vision and pattern recognition*, 1290–1299.

Cheng, B.; Misra, I.; Schwing, A. G.; Kirillov, A.; and Girdhar, R. 2022b. Masked-attention mask transformer for universal image segmentation. In *Proceedings of the IEEE/CVF conference on computer vision and pattern recognition*, 1290–1299.

Cheng, B.; Misra, I.; Schwing, A. G.; Kirillov, A.; and Girdhar, R. 2022c. Masked-attention mask transformer for universal image segmentation. In *Proceedings of the IEEE/CVF conference on computer vision and pattern recognition*, 1290–1299.

Chiang, W.-L.; Li, Z.; Lin, Z.; Sheng, Y.; Wu, Z.; Zhang, H.; Zheng, L.; Zhuang, S.; Zhuang, Y.; Gonzalez, J. E.; Stoica, I.; and Xing, E. P. 2023. Vicuna: An Open-Source Chatbot Impressing GPT-4 with 90%* ChatGPT Quality.

Contributors, X. 2023. XTuner: A Toolkit for Efficiently Fine-tuning LLM. <https://github.com/InternLM/xtuner>.

Ding, H.; Liu, C.; Wang, S.; and Jiang, X. 2021. Vision-language transformer and query generation for referring segmentation. In *Proceedings of the IEEE/CVF international conference on computer vision*, 16321–16330.

Ding, Z.; Wang, J.; and Tu, Z. 2022. Open-vocabulary universal image segmentation with maskclip. *arXiv preprint arXiv:2208.08984*.

Dosovitskiy, A.; Beyer, L.; Kolesnikov, A.; Weissenborn, D.; Zhai, X.; Unterthiner, T.; Dehghani, M.; Minderer, M.; Heigold, G.; Gelly, S.; et al. 2020. An image is worth 16x16 words: Transformers for image recognition at scale. *arXiv preprint arXiv:2010.11929*.

Duan, H.; Yang, J.; Qiao, Y.; Fang, X.; Chen, L.; Liu, Y.; Dong, X.; Zang, Y.; Zhang, P.; Wang, J.; et al. 2024. Vlmevalkit: An open-source toolkit for evaluating large multi-modality models. In *Proceedings of the 32nd ACM International Conference on Multimedia*, 11198–11201.

Fang, Z.; Li, X.; Li, X.; Buhmann, J. M.; Loy, C. C.; and Liu, M. 2023. Explore in-context learning for 3d point cloud understanding. *Advances in Neural Information Processing Systems*, 36: 42382–42395.

Fu, C.; Chen, P.; Shen, Y.; Qin, Y.; Zhang, M.; Lin, X.; Yang, J.; Zheng, X.; Li, K.; Sun, X.; Wu, Y.; and Ji, R. 2024. MME: A Comprehensive Evaluation Benchmark for Multimodal Large Language Models. *arXiv preprint arXiv:2404.08506*.

Gupta, A.; Dollar, P.; and Girshick, R. 2019. Lvis: A dataset for large vocabulary instance segmentation. In *Proceedings of the IEEE/CVF conference on computer vision and pattern recognition*, 5356–5364.

Hudson, D. A.; and Manning, C. D. 2019. Gqa: A new dataset for real-world visual reasoning and compositional question answering. In *Proceedings of the IEEE/CVF conference on computer vision and pattern recognition*, 6700–6709.

Jain, J.; Li, J.; Chiu, M. T.; Hassani, A.; Orlov, N.; and Shi, H. 2023. Oneformer: One transformer to rule universal image segmentation. In *Proceedings of the IEEE/CVF conference on computer vision and pattern recognition*, 2989–2998.

Jia, C.; Yang, Y.; Xia, Y.; Chen, Y.-T.; Parekh, Z.; Pham, H.; Le, Q.; Sung, Y.-H.; Li, Z.; and Duerig, T. 2021. Scaling up visual and vision-language representation learning with noisy text supervision. In *International conference on machine learning*, 4904–4916. PMLR.

Ke, L.; Ye, M.; Danelljan, M.; Tai, Y.-W.; Tang, C.-K.; Yu, F.; et al. 2023. Segment anything in high quality. *Advances in Neural Information Processing Systems*, 36: 29914–29934.

Kembhavi, A.; Salvato, M.; Kolve, E.; Seo, M.; Hajishirzi, H.; and Farhadi, A. 2016. A diagram is worth a dozen images. In *Computer Vision–ECCV 2016: 14th European Conference, Amsterdam, The Netherlands, October 11–14, 2016, Proceedings, Part IV 14*, 235–251. Springer.

Kirillov, A.; He, K.; Girshick, R.; Rother, C.; and Dollár, P. 2019. Panoptic segmentation. In *Proceedings of the IEEE/CVF conference on computer vision and pattern recognition*, 9404–9413.

Kirillov, A.; Mintun, E.; Ravi, N.; Mao, H.; Rolland, C.; Gustafson, L.; Xiao, T.; Whitehead, S.; Berg, A. C.; Lo, W.-Y.; et al. 2023a. Segment anything. In *Proceedings of the IEEE/CVF international conference on computer vision*, 4015–4026.

Kirillov, A.; Mintun, E.; Ravi, N.; Mao, H.; Rolland, C.; Gustafson, L.; Xiao, T.; Whitehead, S.; Berg, A. C.; Lo, W.-Y.; et al. 2023b. Segment anything. In *Proceedings of the IEEE/CVF international conference on computer vision*, 4015–4026.

Lai, X.; Tian, Z.; Chen, Y.; Li, Y.; Yuan, Y.; Liu, S.; and Jia, J. 2024. Lisa: Reasoning segmentation via large language model. In *Proceedings of the IEEE/CVF Conference on Computer Vision and Pattern Recognition*, 9579–9589.

Li, B.; Ge, Y.; Ge, Y.; Wang, G.; Wang, R.; Zhang, R.; and Shan, Y. 2024a. Seed-bench: Benchmarking multimodal large language models. In *Proceedings of the IEEE/CVF Conference on Computer Vision and Pattern Recognition*, 13299–13308.

Li, B.; Weinberger, K. Q.; Belongie, S.; Koltun, V.; and Ranftl, R. 2022a. Language-driven semantic segmentation. *arXiv preprint arXiv:2201.03546*.

Li, B.; Zhang, Y.; Guo, D.; Zhang, R.; Li, F.; Zhang, H.; Zhang, K.; Zhang, P.; Li, Y.; Liu, Z.; et al. 2024b. Llava-onevision: Easy visual task transfer. *arXiv preprint arXiv:2408.03326*.

Li, J.; Li, D.; Xiong, C.; and Hoi, S. 2022b. Blip: Bootstrapping language-image pre-training for unified vision-language understanding and generation. In *International conference on machine learning*, 12888–12900. PMLR.

Li, S.; Ke, L.; Danelljan, M.; Piccinelli, L.; Segu, M.; Van Gool, L.; and Yu, F. 2024c. Matching anything by segmenting anything. In *Proceedings of the IEEE/CVF Conference on Computer Vision and Pattern Recognition*, 18963–18973.

Li, X.; Yuan, H.; Li, W.; Ding, H.; Wu, S.; Zhang, W.; Li, Y.; Chen, K.; and Loy, C. C. 2024d. Omg-seg: Is one model good enough for all segmentation? In *Proceedings of the IEEE/CVF conference on computer vision and pattern recognition*, 27948–27959.

Li, Y.; Du, Y.; Zhou, K.; Wang, J.; Zhao, W. X.; and Wen, J.-R. 2023. Evaluating object hallucination in large vision-language models. *arXiv preprint arXiv:2305.10355*.

Liang, F.; Wu, B.; Dai, X.; Li, K.; Zhao, Y.; Zhang, H.; Zhang, P.; Vajda, P.; and Marculescu, D. 2023. Open-vocabulary semantic segmentation with mask-adapted clip. In *Proceedings of the IEEE/CVF conference on computer vision and pattern recognition*, 7061–7070.

Lin, B.; Ye, Y.; Zhu, B.; Cui, J.; Ning, M.; Jin, P.; and Yuan, L. 2023. Video-llava: Learning united visual representation by alignment before projection. *arXiv preprint arXiv:2311.10122*.

Liu, H.; Li, C.; Li, Y.; and Lee, Y. J. 2024a. Improved baselines with visual instruction tuning. In *Proceedings of the IEEE/CVF Conference on Computer Vision and Pattern Recognition*, 26296–26306.

Liu, H.; Li, C.; Wu, Q.; and Lee, Y. J. 2023a. Visual instruction tuning. *Advances in neural information processing systems*, 36: 34892–34916.

Liu, H.; Li, C.; Wu, Q.; and Lee, Y. J. 2023b. Visual instruction tuning. *Advances in neural information processing systems*, 36: 34892–34916.

Liu, Y.; Duan, H.; Zhang, Y.; Li, B.; Zhang, S.; Zhao, W.; Yuan, Y.; Wang, J.; He, C.; Liu, Z.; et al. 2024b. Mmbench: Is your multi-modal model an all-around player? In *European conference on computer vision*, 216–233. Springer.

Loshchilov, I.; and Hutter, F. 2017. Decoupled weight decay regularization. *arXiv preprint arXiv:1711.05101*.

Pan, T.; Tang, L.; Wang, X.; and Shan, S. 2024. Tokenize anything via prompting. In *European Conference on Computer Vision*, 330–348. Springer.

Peng, Z.; Wang, W.; Dong, L.; Hao, Y.; Huang, S.; Ma, S.; and Wei, F. 2023. Kosmos-2: Grounding multimodal large language models to the world. *arXiv preprint arXiv:2306.14824*.

Qi, L.; Kuen, J.; Guo, W.; Shen, T.; Gu, J.; Jia, J.; Lin, Z.; and Yang, M.-H. 2022a. High-quality entity segmentation. *arXiv preprint arXiv:2211.05776*.

Qi, L.; Kuen, J.; Wang, Y.; Gu, J.; Zhao, H.; Torr, P.; Lin, Z.; and Jia, J. 2022b. Open world entity segmentation. *IEEE Transactions on Pattern Analysis and Machine Intelligence*, 45(7): 8743–8756.

Radford, A.; Kim, J. W.; Hallacy, C.; Ramesh, A.; Goh, G.; Agarwal, S.; Sastry, G.; Askell, A.; Mishkin, P.; Clark, J.; et al. 2021. Learning transferable visual models from natural language supervision. In *International conference on machine learning*, 8748–8763. PMLR.

Rajić, F.; Ke, L.; Tai, Y.-W.; Tang, C.-K.; Danelljan, M.; and Yu, F. 2025. Segment anything meets point tracking. In *2025 IEEE/CVF Winter Conference on Applications of Computer Vision (WACV)*, 9302–9311. IEEE.

Rasheed, H.; Maaz, M.; Shaji, S.; Shaker, A.; Khan, S.; Cholakkal, H.; Anwer, R. M.; Xing, E.; Yang, M.-H.; and Khan, F. S. 2024. Glamm: Pixel grounding large multimodal model. In *Proceedings of the IEEE/CVF Conference on Computer Vision and Pattern Recognition*, 13009–13018.

Ravi, N.; Gabeur, V.; Hu, Y.-T.; Hu, R.; Ryali, C.; Ma, T.; Khedr, H.; Rädle, R.; Rolland, C.; Gustafson, L.; et al. 2024. Sam 2: Segment anything in images and videos. *arXiv preprint arXiv:2408.00714*.

Ren, Z.; Huang, Z.; Wei, Y.; Zhao, Y.; Fu, D.; Feng, J.; and Jin, X. 2024. Pixellm: Pixel reasoning with large multimodal model. In *Proceedings of the IEEE/CVF Conference on Computer Vision and Pattern Recognition*, 26374–26383.

Touvron, H.; Lavril, T.; Izacard, G.; Martinet, X.; Lachaux, M.-A.; Lacroix, T.; Rozière, B.; Goyal, N.; Hambro, E.; Azhar, F.; et al. 2023. Llama: Open and efficient foundation language models. *arXiv preprint arXiv:2302.13971*.

Tschannen, M.; Gritsenko, A.; Wang, X.; Naeem, M. F.; Alabdulmohsin, I.; Parthasarathy, N.; Evans, T.; Beyer, L.; Xia, Y.; Mustafa, B.; et al. 2025. Siglip 2: Multilingual vision-language encoders with improved semantic understanding, localization, and dense features. *arXiv preprint arXiv:2502.14786*.

VS, V.; Borse, S.; Park, H.; Das, D.; Patel, V.; Hayat, M.; and Porikli, F. 2024. PosSAM: Panoptic Open-vocabulary Segment Anything. *arXiv:2403.09620*.

Wang, H.; Wang, W.; and Liu, J. 2021a. Temporal memory attention for video semantic segmentation. In *2021 IEEE International Conference on Image Processing (ICIP)*, 2254–2258. IEEE.

Wang, H.; Zhu, Y.; Adam, H.; Yuille, A.; and Chen, L.-C. 2021b. Max-deeplab: End-to-end panoptic segmentation with mask transformers. In *Proceedings of the IEEE/CVF conference on computer vision and pattern recognition*, 5463–5474.

Wang, X.; Zhang, X.; Cao, Y.; Wang, W.; Shen, C.; and Huang, T. 2023. Seggpt: Segmenting everything in context. *arXiv preprint arXiv:2304.03284*.

Wang, Z.; Lu, Y.; Li, Q.; Tao, X.; Guo, Y.; Gong, M.; and Liu, T. 2022. Cris: Clip-driven referring image segmentation. In *Proceedings of the IEEE/CVF conference on computer vision and pattern recognition*, 11686–11695.

Wei, C.; Tan, H.; Zhong, Y.; Yang, Y.; and Ma, L. 2024a. Lasagna: Language-based segmentation assistant for complex queries. *arXiv preprint arXiv:2404.08506*.

Wei, C.; Zhong, Y.; Tan, H.; Liu, Y.; Zhao, Z.; Hu, J.; and Yang, Y. 2024b. HyperSeg: Towards Universal Visual Segmentation with Large Language Model. *arXiv preprint arXiv:2411.17606*.

Xu, J.; Liu, S.; Vahdat, A.; Byeon, W.; Wang, X.; and De Mello, S. 2023. Open-vocabulary panoptic segmentation with text-to-image diffusion models. In *Proceedings of the IEEE/CVF Conference on Computer Vision and Pattern Recognition*, 2955–2966.

Xu, K.; Ba, J.; Kiros, R.; Cho, K.; Courville, A.; Salakhudinov, R.; Zemel, R.; and Bengio, Y. 2015. Show, attend and tell: Neural image caption generation with visual attention. In *International conference on machine learning*, 2048–2057. PMLR.

Xu, S.; Yuan, H.; Shi, Q.; Qi, L.; Wang, J.; Yang, Y.; Li, Y.; Chen, K.; Tong, Y.; Ghanem, B.; et al. 2024. Rapsam: Towards real-time all-purpose segment anything. *arXiv preprint arXiv:2401.10228*.

Yan, B.; Jiang, Y.; Wu, J.; Wang, D.; Luo, P.; Yuan, Z.; and Lu, H. 2023. Universal instance perception as object discovery and retrieval. In *Proceedings of the IEEE/CVF Conference on Computer Vision and Pattern Recognition*, 15325–15336.

You, H.; Zhang, H.; Gan, Z.; Du, X.; Zhang, B.; Wang, Z.; Cao, L.; Chang, S.-F.; and Yang, Y. 2023. Ferret: Refer and ground anything anywhere at any granularity. *arXiv preprint arXiv:2310.07704*.

Yu, L.; Lin, Z.; Shen, X.; Yang, J.; Lu, X.; Bansal, M.; and Berg, T. L. 2018. Mattnet: Modular attention network for referring expression comprehension. In *Proceedings of the IEEE conference on computer vision and pattern recognition*, 1307–1315.

Yuan, H.; Li, X.; Zhang, T.; Huang, Z.; Xu, S.; Ji, S.; Tong, Y.; Qi, L.; Feng, J.; and Yang, M.-H. 2025. Sa2VA: Marrying

SAM2 with LLaVA for Dense Grounded Understanding of Images and Videos. *arXiv preprint arXiv:2501.04001*.

Yuan, H.; Li, X.; Zhou, C.; Li, Y.; Chen, K.; and Loy, C. C. 2024a. Open-vocabulary SAM: Segment and recognize twenty-thousand classes interactively. In *European Conference on Computer Vision*, 419–437. Springer.

Yuan, Y.; Li, W.; Liu, J.; Tang, D.; Luo, X.; Qin, C.; Zhang, L.; and Zhu, J. 2024b. Osprey: Pixel understanding with visual instruction tuning. In *Proceedings of the IEEE/CVF Conference on Computer Vision and Pattern Recognition*, 28202–28211.

Zhai, X.; Mustafa, B.; Kolesnikov, A.; and Beyer, L. 2023. Sigmoid loss for language image pre-training. In *Proceedings of the IEEE/CVF international conference on computer vision*, 11975–11986.

Zhang, T.; Li, X.; Fei, H.; Yuan, H.; Wu, S.; Ji, S.; Loy, C. C.; and Yan, S. 2024a. Omg-llava: Bridging image-level, object-level, pixel-level reasoning and understanding. *Advances in Neural Information Processing Systems*, 37: 71737–71767.

Zhang, T.; Li, X.; Fei, H.; Yuan, H.; Wu, S.; Ji, S.; Loy, C. C.; and Yan, S. 2024b. Omg-llava: Bridging image-level, object-level, pixel-level reasoning and understanding. *Advances in Neural Information Processing Systems*, 37: 71737–71767.

Zhang, W.; Pang, J.; Chen, K.; and Loy, C. C. 2021. K-net: Towards unified image segmentation. *Advances in Neural Information Processing Systems*, 34: 10326–10338.

Zhang, Z.; Ma, Y.; Zhang, E.; and Bai, X. 2024c. Psalm: Pixelwise segmentation with large multi-modal model. In *European Conference on Computer Vision*, 74–91. Springer.

Zhou, K.; Yang, J.; Loy, C. C.; and Liu, Z. 2022a. Learning to prompt for vision-language models. *International Journal of Computer Vision*, 130(9): 2337–2348.

Zhou, Q.; Li, X.; He, L.; Yang, Y.; Cheng, G.; Tong, Y.; Ma, L.; and Tao, D. 2022b. TransVOD: End-to-end video object detection with spatial-temporal transformers. *IEEE Transactions on Pattern Analysis and Machine Intelligence*, 45(6): 7853–7869.

Zou, X.; Dou, Z.-Y.; Yang, J.; Gan, Z.; Li, L.; Li, C.; Dai, X.; Behl, H.; Wang, J.; Yuan, L.; et al. 2023a. Generalized decoding for pixel, image, and language. In *Proceedings of the IEEE/CVF conference on computer vision and pattern recognition*, 15116–15127.

Zou, X.; Yang, J.; Zhang, H.; Li, F.; Li, L.; Wang, J.; Wang, L.; Gao, J.; and Lee, Y. J. 2023b. Segment everything everywhere all at once. *Advances in neural information processing systems*, 36: 19769–19782.

Technical Appendices and Supplementary Material

In the Appendix, we first provide more details on the dataset, model architecture, and implementation of the proposed method. Then, we present additional experimental results on more benchmarks to demonstrate the effectiveness of our approach. Next, we include ablation studies on dataset balance resampling and the image encoder. Following that, we provide further visualization results for different tasks. Finally, we discuss the limitations and future work.

More Dataset Details

Training Datasets. In Table 10, we show the datasets used in our multi-stage training. For the segmentor fine-tuning stage, we fine-tune the segmentor on generic segmentation datasets. For the alignment pre-training stage, we pre-train the dual projectors on the alignment LLaVA 558K (Liu et al. 2023b) dataset. For the mixed fine-tuning stage, we fine-tune the whole model on mixed datasets, including both segmentation and conversation datasets. There are six types of datasets in total, including one image-level dataset and five segmentation datasets.

Building COCO-VGD Dataset. The COCO-VGD dataset is built on the images and annotations of the COCO2017 instance segmentation dataset, which provides instance-level segmentation masks for each object in an image. We automatically generate four types of visual prompts: point, scribe, box, and mask, for each instance in the image, following (Zhang et al. 2024c). We randomly sample one type of visual prompt for each category as the visually grounded prompt during training and evaluation.

Dataset Balance Resampling. As shown in Table 10, the dataset sizes vary, ranging from 0.2K to 665K. The data ratio among the datasets is crucial to the model’s performance during mixed fine-tuning. To balance the different dataset sizes, we propose a dataset balance resampling strategy following (Gupta et al. 2019). For each dataset d , let f_d be the frequency of dataset d in the mixed datasets. We define the dataset-level repeat factor as $r_d = \max(1, \sqrt{t/f_d})$, where t is a hyperparameter controlling the oversampling ratio. We then repeat dataset d with a repeat factor of r_d .

More Model Details

Model Framework. For the segmentor, we adopt SAM-L (Ke et al. 2023) as the segmentation encoder and the Mask2Former head (Cheng et al. 2022a) as the decoder. To reduce the number of connector parameters, we employ a bottleneck architecture, which first reduces the dimension of the segmentation feature to 512 via a 1×1 convolution, then further refines the feature via a 3×3 convolution, and finally expands the dimension to a value determined by the spatial scale of the pixel shuffle (Chen et al. 2024) operation using another 1×1 convolution. For the MLLM, we use SigLIP2-so400m (Tschannen et al. 2025) as the image encoder, an MLP as the image projector, another MLP with a pixel shuffle operation as the segmentation projector, and Phi-3-mini-4k-instruct (Abdin et al. 2024) as the LLM. The total number of parameters in X-SAM is about 5B.

Region Sampling. To sample region features from the vision query, we adopt the region sampling strategy from (You et al. 2023). Specifically, we first convert the vision query into a binary mask, then perform point sampling on the segmentor-encoded features to obtain the region features, and finally apply mean pooling to produce the final region features. These region features are placed in the corresponding position of `<region>` in the language instruction, serving as vision query categories for the segmentation decoder.

More Training Details

Stage 1: Segmentor Fine-tuning. During segmentor fine-tuning, we unfreeze all parameters of the segmentor, including the SAM encoder, segmentation connector, and segmentation decoder. The learning rate is set to 1e-4 for all components except the segmentation encoder, which uses a learning rate of 1e-5. We set the batch size to 64 and train for 36 epochs. The SAM encoder is initialized with pre-trained weights, while the segmentation connector and decoder are initialized with random weights. Additionally, we apply random scale augmentation to the images during training, with a scale of [0.1, 2.0].

Stage 2: Alignment Pre-training. During alignment pre-training, we train only the parameters of the dual projectors and keep all other parameters fixed. The learning rate is set to 1e-3, and the batch size is set to 256. The dual projectors are initialized with random weights, the segmentation encoder is initialized with the pre-trained weights from the segmentor fine-tuning stage, and the image encoder and LLM are initialized with their official pre-trained weights. Training is conducted for 1 epoch.

Stage 3: Mixed Fine-tuning. During mixed fine-tuning, we fine-tune all parameters of the model. The learning rate for the dual encoders is set to 4e-6, while the learning rate for the other modules is set to 4e-5. The batch size is set to 64, and training is conducted for 1 epoch. The segmentation encoder, segmentation connector, and segmentation decoder are initialized with pre-trained weights from the segmentor fine-tuning stage, and the image encoder is initialized with official pre-trained weights. The dual projectors are initialized with pre-trained weights from the alignment pre-training stage. Additionally, to make training more stable, we ensure that all data within a global batch come from the same source.

The hyper-parameters in the multi-stage training are shown in Table 11. A simplified illustration of the multi-stage training is shown in Figure 5.

More Evaluation Details

PSALM COCO-VGD Evaluation. PSALM (Zhang et al. 2024c) is a segmentation MLLM that supports generic segmentation, open-vocabulary segmentation, referring segmentation, interactive segmentation, and more. To evaluate its performance on our proposed COCO-VGD dataset, we follow the same evaluation process as for X-SAM. We randomly sample some instance annotations, as done with X-SAM, and then feed them to PSALM to obtain instance-level predictions. PSALM is trained on the COCO-Interactive dataset, which shares the same source as COCO-VGD but

Task	Datasets	# Sample
Generic Segmentation	Stage 1: Segmentor Fine-tuning COCO Panoptic (Kirillov et al. 2019) (118K)	118K
Image Conversation	Stage 2: Alignment Pre-training LLaVA (Liu et al. 2023b) (558k)	558k
Image Conversation	Stage 3: Mixed Fine-tuning LLaVA-1.5 (Liu et al. 2023b) (665K)	665K
Generic Segmentation	COCO Panoptic (Kirillov et al. 2019) (118K)	118K
VGD Segmentation	COCO-VGD (117K)	117K
Referring Segmentation	RefCOCO(17K), RefCOCO+(17K), RefCOCOOG(22K)	301K
GCG Segmentation	Grand-f (Rasheed et al. 2024) (1K), RefCOCOOG (19K), PSG (28K), Flickr (148K)	195K
Reasoning Segmentation	LISA ReasonSeg (Lai et al. 2024) (0.2K)	0.2K

Table 10: The Datasets Specification. The datasets used in multi-stage training. # Sample is the total number of samples in this task.

Item	Stage 1	Stage 2	Stage 3
	Segmentor Fine-tuning	Alignment Pre-training	Mixed Fine-tuning
batch size	64	256	64
training epochs	36	1	1
lr of dual encoders	1e-5	-	4e-6
lr of other modules	1e-4	1e-3	4e-5
optimizer	AdamW (Loshchilov et al. 2017)		
optimizer momentum	$\beta_1 = 0.9, \beta_2 = 0.999$		
weight decay	0.05	0	0.05
warmup ratio	0.03	0.03	0.03
clip max norm	0.01	1	1
image augmentation	random scale[0.1, 2.0]	-	-

Table 11: The Hyper-parameters in Multi-stage Training of X-SAM.

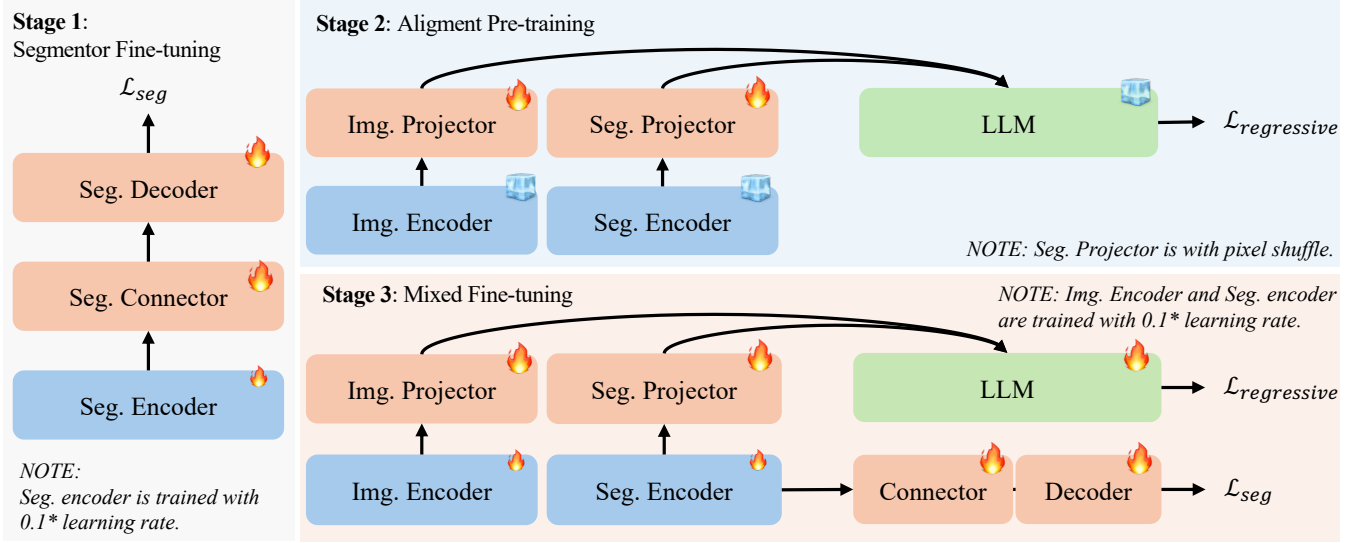


Figure 5: The Multi-stage Training of X-SAM. X-SAM performs a multi-stage training process, including segmentor fine-tuning, alignment pre-training, and mixed fine-tuning. *Segmentor fine-tuning*: train the segmentor on the segmentation datasets to obtain a generalized segmentor. *Alignment pre-training*: train the dual projectors to align the vision features and the LLM features. *Mixed fine-tuning*: fine-tune the dual projectors, the segmentation decoder, and the LLM on the mixed datasets.

Method	Encoder	PQ	AP	mIoU
Mask2Former(Cheng et al. 2022a)	Swin-L	57.8	48.6	67.4
X-Decoder(Zou et al. 2023a)	DaViT-B	56.2	45.8	66.0
SEEM(Zou et al. 2023b)	DaViT-B	56.1	46.4	66.3
OMG-LLaVA(Zhang et al. 2024a)	ConvNeXt-XXL	53.8	-	-
PSALM(Zhang et al. 2024c)	Swin-B	55.9	45.7	66.6
X-SAM (Ours)	SAM-L	54.7	47.0	66.5

Table 12: Comparison of Generic Segmentation. We compare different methods on the generic segmentation benchmarks.

Method	PQ	AP	mIoU
MaskCLIP (Ding et al. 2022)	15.1	6.0	23.7
ODISE(Xu et al. 2023)	22.6	14.4	29.9
PSALM(Zhang et al. 2024c)	13.7	9.0	18.2
HyperSeg(Wei et al. 2024b)	<u>16.1</u>	-	<u>22.3</u>
X-SAM (Ours)	20.9	16.2	28.8

Table 13: Comparison of OV Segmentation. We compare different methods on the A150-OV segmentation benchmarks.

Method	val		test					
	overall		short query		long query		overall	
	gIoU	cIoU	gIoU	cIoU	gIoU	cIoU	gIoU	cIoU
OVSeg (Liang et al. 2023)	28.5	18.6	18.0	15.5	28.7	22.5	26.1	20.8
SEEM (Zou et al. 2023b)	25.5	21.2	20.1	11.5	25.6	20.8	24.3	18.7
LISA-7B (Lai et al. 2024)	44.4	46.0	37.6	34.4	36.6	34.7	36.8	34.1
LISA-7B (ft) (Lai et al. 2024)	<u>52.9</u>	54.0	<u>40.6</u>	<u>40.6</u>	<u>49.4</u>	51.0	<u>47.3</u>	48.4
X-SAM (Ours)	56.6	32.9	47.7	48.1	56.0	<u>40.8</u>	57.8	41.0

Table 14: Comparison of Reasoning Segmentation. We compare X-SAM with other methods on the reasoning segmentation benchmark.

Method	Point		Scribble		Box		Mask	
	mIoU	cIoU	mIoU	cIoU	mIoU	cIoU	mIoU	cIoU
SAM-B(Kirillov et al. 2023a)	48.7	33.6	-	-	73.7	68.7	-	-
SAM-L(Kirillov et al. 2023a)	51.8	37.7	-	-	76.6	71.6	-	-
SEEM-B(Zou et al. 2023b)	47.8	57.8	43.0	44.0	44.9	42.1	48.4	65.0
OMG-Seg(Li et al. 2024d)	59.3	-	-	-	-	-	-	-
PSALM(Zhang et al. 2024c)	<u>64.3</u>	74.0	66.9	80.0	<u>67.3</u>	80.9	<u>67.6</u>	82.4
X-SAM (Ours)	65.4	<u>62.9</u>	66.9	<u>75.7</u>	69.6	<u>75.4</u>	69.7	<u>77.0</u>

Table 15: Comparison of Interactive Segmentation. We compare X-SAM with other methods on the interactive segmentation benchmark.

performs classification for each interactive visual prompt. As a result, the AP metric for VGD segmentation is poor because the instance-level predictions are of low quality. This may explain why PSALM lacks the capability for instance-level visual grounding segmentation.

X-SAM COCO-Interactive Evaluation. X-SAM is the first unified segmentation MLLM, capable of adapting to all image segmentation tasks, including interactive segmentation (Zhang et al. 2024c). To evaluate its performance on the COCO-Interactive dataset, we first filter the instance-level predictions using a threshold of 0.5. We then calculate the IoU score between each remaining prediction and the visual prompt mask. Finally, we select the instance prediction with the highest IoU score as the final interactive segmentation result.

More Experimental Results

Generic Segmentation. Table 12 presents the results of generic segmentation. Thanks to our segmentor design and

fine-tuning, X-SAM can adapt to generic segmentation and achieves competitive performance on the COCO-Panoptic dataset.

Open-Vocabulary Segmentation. Table 13 shows the results of open-vocabulary segmentation. Benefiting from the robust mask generation of SAM and our mixed fine-tuning strategy, X-SAM achieves the best performance on open-vocabulary segmentation tasks.

Reasoning Segmentation. In Table 14, we present the results of reasoning segmentation on the reasoning segmentation benchmark. We report the performance of our method on both the validation set and the test set, following (Lai et al. 2024). X-SAM achieves the best gIoU metric on both the validation and test sets, even though it is not specifically designed for reasoning segmentation. While the cIoU metric is not the best, it remains comparable to state-of-the-art methods. As the number of samples in the validation and test sets is limited, the results on this benchmark may not be stable.

	LLM	Zero-Shot	val		testA		testB	
			cIoU	gIoU	cIoU	gIoU	cIoU	gIoU
MattNet (Yu et al. 2018)	-	✗	47.5	48.2	58.7	59.3	45.3	46.1
LTS (Ding et al. 2021)	-	✗	52.3	52.7	61.9	62.6	49.9	50.4
CRIS (Wang et al. 2022)	-	✗	55.3	-	63.8	-	51.0	-
LISA (Lai et al. 2024)	Vicuna-7B	✗	38.7	32.2	52.6	48.5	44.8	39.7
X-SAM(Ours)	Phi3-3.8B	✓	36.9	44.8	32.3	34.5	36.4	38.9

Table 16: Comparison of Generalized Referring Segmentation. We compare X-SAM with other methods on the gRefCOCO benchmark.

Method	Encoder	# Params.	Epochs	PQ	PQ Th	PQ St	AP Th _{pan}	mIoU ^{pan}
Max-DeepLab(Wang et al. 2021b)	Max-L	451M	216	51.1	57.0	42.2	-	-
MaskFormer(Cheng et al. 2022c)	Swin-L	212M	300	52.7	58.5	44.0	40.1	64.8
K-Net(Zhang et al. 2021)	Swin-L	-	36	54.6	60.2	46.0	-	-
Mask2Former(Cheng et al. 2022a)	Swin-L	216M	100	57.8	64.2	48.1	48.6	67.4
X-SAM (Ours)	SAM-L	364M	36	54.2	60.0	45.4	44.2	63.8

Table 17: Comparison of Closed-set Segmentation. We compare X-SAM with other methods on the COCO-Panoptic benchmark.

Method	MME	MMBench	SEED-Bench	POPE	AI2D
LLaVA-1.5 (Liu et al. 2024a)	1510 / -	64.3	58.6	87.3	-
LLaVA-OV (Li et al. 2024b)	1580 / 418	80.8	75.4	-	81.4
LISA (Lai et al. 2024)	1 / 1	0.4	-	0.0	0.0
PixelLM (Ren et al. 2024)	309 / 135	17.4	-	0.0	0.0
LaSagnA (Wei et al. 2024a)	0 / 0	0.0	-	0.0	0.0
GLaMM (Rasheed et al. 2024)	14 / 9	36.8	-	0.94	28.2
OMG-LLaVA (Zhang et al. 2024a)	1177 / 235	47.9	56.5	80.0	42.9
X-SAM (Ours)	1374 / 312	69.3	69.3	89.3	62.6

Table 18: Comparison of Image-level Benchmarks. We compare X-SAM with other methods on the image-level benchmarks, including MME (Fu et al. 2024), MMBench (Liu et al. 2024b), SEED-Bench (Li et al. 2024a), POPE (Li et al. 2023), and AI2D (Kembhavi et al. 2016).

Generalized Referring Segmentation. In Table 16, we present the results of generalized referring segmentation on the gRefCOCO benchmark. We report the performance of our method on both the validation set and the test set, following (Yu et al. 2018). X-SAM achieves the comparable performance to state-of-the-art methods under zero-shot setting, it will achieve better performance with the fine-tuning on the gRefCOCO dataset.

Interactive Segmentation. Table 15 shows the results of the interactive segmentation. Since interactive segmentation shares similar data with VGD segmentation, we exclude the training data for interactive segmentation and perform a process similar to that used for VGD segmentation to obtain the interactive segmentation results. X-SAM achieves the best or second-best performance on interactive segmentation, even without being trained on the specific data.

Closed-Set Segmentation. In Table 17, we present the results of segmentor fine-tuning on the closed-set COCO-Panoptic benchmark. To preserve the robust generalization

ability of SAM in mask prediction, we fine-tune the SAM encoder for only 36 epochs. Compared with other methods, our approach achieves comparable performance to the SAM-L encoder with just 36 epochs of fine-tuning without any complex data augmentation.

Image-level Benchmarks. In Table 18, we present the results of image-level benchmarks, including MME (Fu et al. 2024), MMBench (Liu et al. 2024b), SEED-Bench (Li et al. 2024a), POPE (Li et al. 2023), and AI2D (Kembhavi et al. 2016). When jointly co-training with segmentation and conversation datasets, X-SAM achieves the best performance compared to other segmentation MLLMs on these benchmarks. Compared to LISA (Lai et al. 2024), PixelLM (Ren et al. 2024), and GLaMM (Rasheed et al. 2024), our method achieves significant improvements, demonstrating its effectiveness—even outperforming the previous best, OMG-LLaVA (Zhang et al. 2024a). On the POPE benchmark, X-SAM even surpasses LLaVA-V1.5 (Liu et al. 2023b), which is designed specifically for image-level conversation.

t	COCO-Pan PQ	A150-OV PQ	RefCOCO cIoU	Reason-Val gIoU	GCG-Val mIoU	COCO-VGD AP	Conv.-MMB Acc	$\sum \Delta$
0	53.5	20.6	84.2	44.1	62.8	47.4	68.6	0.0
0.001	53.9	<u>20.9</u>	85.5	44.1	62.7	47.7	67.3	$\uparrow 0.9$
0.01	54.3	21.0	84.6	<u>46.5</u>	<u>63.1</u>	48.1	67.4	$\uparrow 3.8$
0.1	54.7	<u>20.9</u>	85.1	56.6	69.4	47.9	69.3	$\uparrow 22.7$

Table 19: Ablation of Dataset Balance Resampling. $\sum \Delta$ represents the total performance improvement compared to the first row.

Img. Enc.	COCO-Pan PQ	A150-OV PQ	RefCOCO cIoU	Reason-Val gIoU	GCG-Val mIoU	COCO-VGD AP	Conv.-MME Acc	Conv.-MMB Acc
CLIP (Radford et al. 2021)	<u>53.7</u>	<u>21.2</u>	<u>84.8</u>	55.6	<u>62.6</u>	48.0	1327 / 277	68.5
SigLIP (Zhai et al. 2023)	53.2	21.7	83.3	61.6	61.8	48.0	1331 / 280	68.4
SigLIP2 (Tschannen et al. 2025)	54.7	20.9	85.1	<u>56.6</u>	69.4	47.9	1374 / 312	69.3

Table 20: Ablation of Image Encoder. We ablate the impact of different image encoders, including CLIP (Radford et al. 2021), SigLIP (Zhai et al. 2023), and SigLIP2 (Tschannen et al. 2025), on the performance of X-SAM.

LLM	COCO-Pan PQ	COCO-VGD AP	Conv.-MMB Acc
Phi3-3.8B (Abdin et al. 2024)	54.7	47.9	69.3
Qwen3-1.7B (Bai et al. 2023)	54.3	47.8	65.8
Vicuna-7B (Chiang et al. 2023)	54.5	47.3	71.3

Table 21: Ablation of LLMs. We ablate the performance of X-SAM with different LLMs.

Seg Data	Conv.-MME	SEED	POPE	AI2D
	Acc	Acc	Acc	Acc
\times	1397 / 332	69.0	87.6	64.8
\checkmark	1374 / 312	69.3	89.3	62.6

Table 22: Ablation of Segmentation Data. We ablate the performance of X-SAM with and without segmentation data on the image-level benchmarks.

More Ablation Studies

Dataset Balance Resampling. In Table 19, we ablate the oversampling ratio t from 0 to 0.1 in dataset balance resampling. When $t = 0$, no dataset is oversampled. Otherwise, datasets are oversampled with a repeat factor of $r_d = \max(1, \sqrt{t/f_d})$. We find that the performance on some small datasets is sensitive to the oversampling ratio t , especially for the reasoning segmentation dataset, where the gIoU score improves from 44.1% to 56.6% as t increases from 0 to 0.1. Meanwhile, larger datasets are not sensitive to the oversampling ratio t . As a result, the overall performance improvement reaches its highest when $t = 0.1$. Therefore, we set t to 0.1 in the final experiment.

Image Encoder. In Table 20, we ablate the image encoder of X-SAM by replacing it with CLIP (Radford et al. 2021), SigLIP-so400m (Zhai et al. 2023), and SigLIP2-so400m (Tschannen et al. 2025). It can be observed that using more powerful image encoders improves the image content understanding ability of X-SAM, especially on the image conversation and GCG segmentation benchmarks, and even enhances performance on the generic segmentation benchmark. Although SigLIP achieves the best performance on the reasoning segmentation benchmark, it does not have a performance advantage on the other benchmarks. Meanwhile, SigLIP2 demonstrates more robust and consistently better performance across all benchmarks. Therefore, we

adopt SigLIP2-so400m as the image encoder for the final experiment.

LLM. In Table 21, we ablate the LLM of X-SAM with different LLMs. We find that Phi3-3.8B (Abdin et al. 2024) achieves the best performance on the COCO-Pan and COCO-VGD benchmarks, while Vicuna-7B (Chiang et al. 2023) achieves the best performance on the Conv.-MMB benchmark. Moreover, Phi3-3.8B show more robust and consistent performance across segmentation benchmarks, we adopt it as the LLM for the final experiment.

Segmentation Data. In Table 22, we ablate the impact of segmentation data on the image-level benchmarks. We find that adding segmentation data improves the performance of X-SAM on the image-level benchmarks, especially on the hallucination-prone benchmarks, such as SEED and POPE.

More Visualization Results

Generic Segmentation. Figure 6 shows the visualization results of X-SAM in generic segmentation, including semantic, instance and panoptic segmentation, which needs both the semantic and instance level understanding of the image. X-SAM can generate accurate and complete masks for the objects in the image.

Open-Vocabulary Segmentation. Figure 7 shows the visualization results of X-SAM in open-vocabulary (OV) segmentation, including OV-semantic, OV-instance, and OV-panoptic segmentation, which require segmenting objects

that may not exist in the training set. X-SAM can segment objects that are not in the training set, demonstrating the robust generalization ability of the proposed method.

GCG Segmentation. Figure 8 shows the visualization results of X-SAM in GCG segmentation, which needs to describe the image and output the corresponding mask. X-SAM can not only effectively understand the image and generate the language description, but also generate the segmentation masks for the corresponding phrases.

Referring Segmentation. Figure 9 shows the visualization results of X-SAM in referring segmentation, which needs to segment objects that are referred to by natural language. X-SAM can effectively understand the referring expression and segment the objects that are referred to by natural language.

Reasoning Segmentation. Figure 10 shows the visualization results of X-SAM in reasoning segmentation, which needs to segment the object that is related to the question. X-SAM can effectively understand the complex question and then generate the corresponding mask for the question.

Interactive Segmentation. Figure 11 shows the visualization results of X-SAM in interactive segmentation, which needs to segment the individual objects with which the user interacts. X-SAM can generate the corresponding mask for the user’s interactive visual prompt.

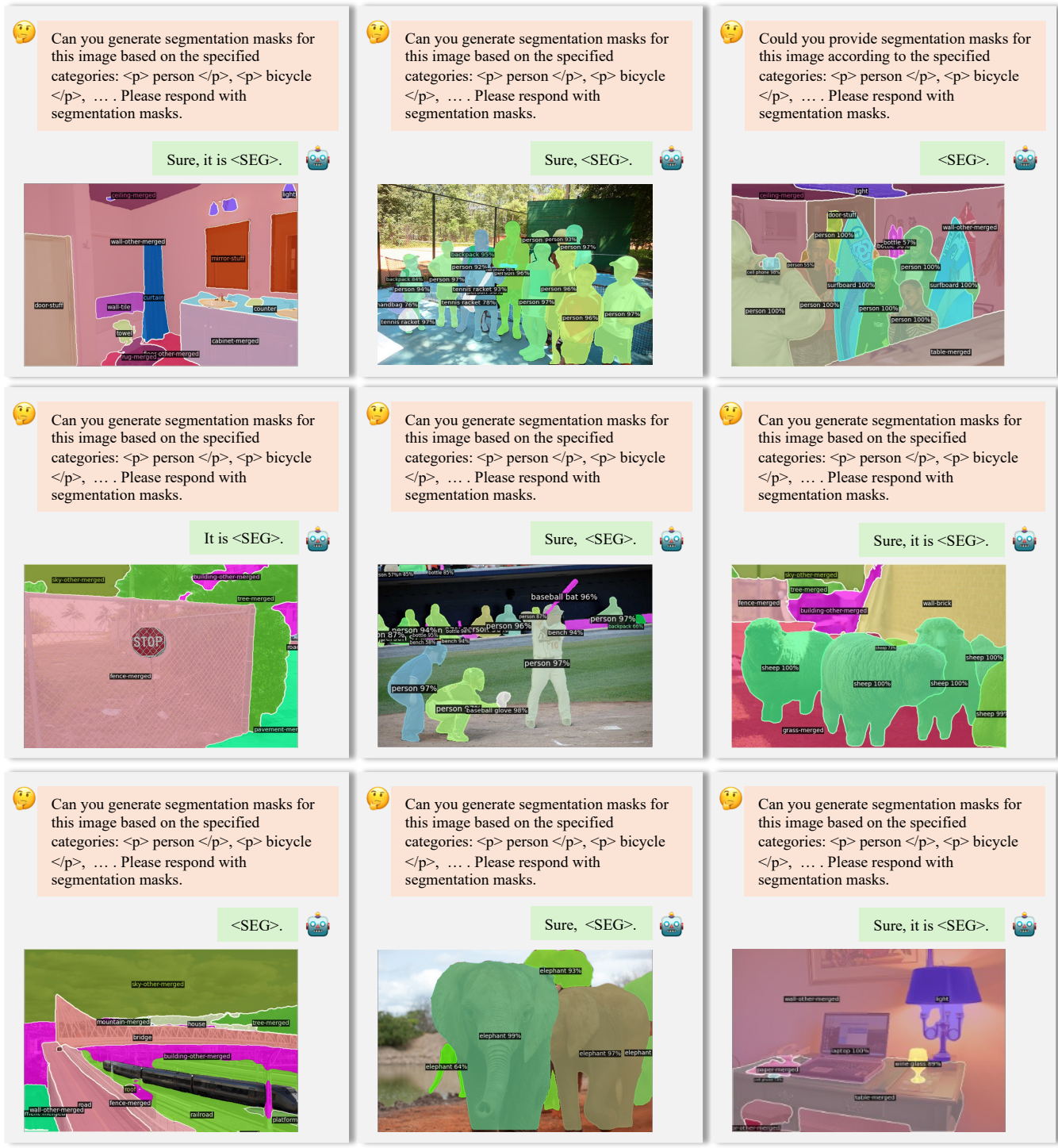
VGD Segmentation. Figure 12 shows the visualization results of X-SAM in VGD segmentation for a single image, which needs to segment all the objects in the *single image* that is grounded with the user’s visual prompt. X-SAM can effectively segment all the objects in the image given by the user’s visual grounded prompt. In addition, X-SAM can perform VGD segmentation on the *cross image*, which needs to segment the objects grounded in another image. Figure 13 shows the visualization results of X-SAM in VGD segmentation for cross image, which demonstrates the effectiveness of X-SAM for VGD segmentation both in single image and cross image.

Further Discussions

Limitation. Although X-SAM achieves unified segmentation by extending *segment anything* to *any segmentation*, there is still considerable room for improvement. First, joint co-training with segmentation datasets and conversation datasets negatively impacts performance on some segmentation datasets, a phenomenon also observed in (Zhang et al. 2024a) and (Rasheed et al. 2024). This challenge may be addressed by designing a more balanced dataset mixture. Second, the performance of X-SAM is not optimal across all tasks, which has also been observed in other unified segmentation methods (Zhang et al. 2024a; Rasheed et al. 2024; Lai et al. 2024). This challenge remains a major obstacle for unified models and may be addressed by scaling up the model size and the amount of training data.

Future Work. Several avenues for future work can be explored with our novel unified framework. We highlight two potential directions. The first is to integrate X-SAM with SAM2 (Ravi et al. 2024), a unified model for segmentation in images and videos. This integration would further extend the application of X-SAM to video segmentation. The second direction is to extend VGD segmentation to the

video domain, which would constitute an interesting video segmentation task and introduce visually grounded temporal information to segmentation. We plan to explore these directions in the future, provided that more computational resources become available.



Semantic

Instance

Panoptic

Figure 6: Visualization Results of Generic Segmentation. Visualized images are sampled from the COCO2017 Val set. More category names are omitted for better visualization.



Figure 7: Visualization Results of Open-Vocabulary (OV) Segmentation. Visualized images are sampled from the ADE20K Val set. More category names are omitted for better visualization.

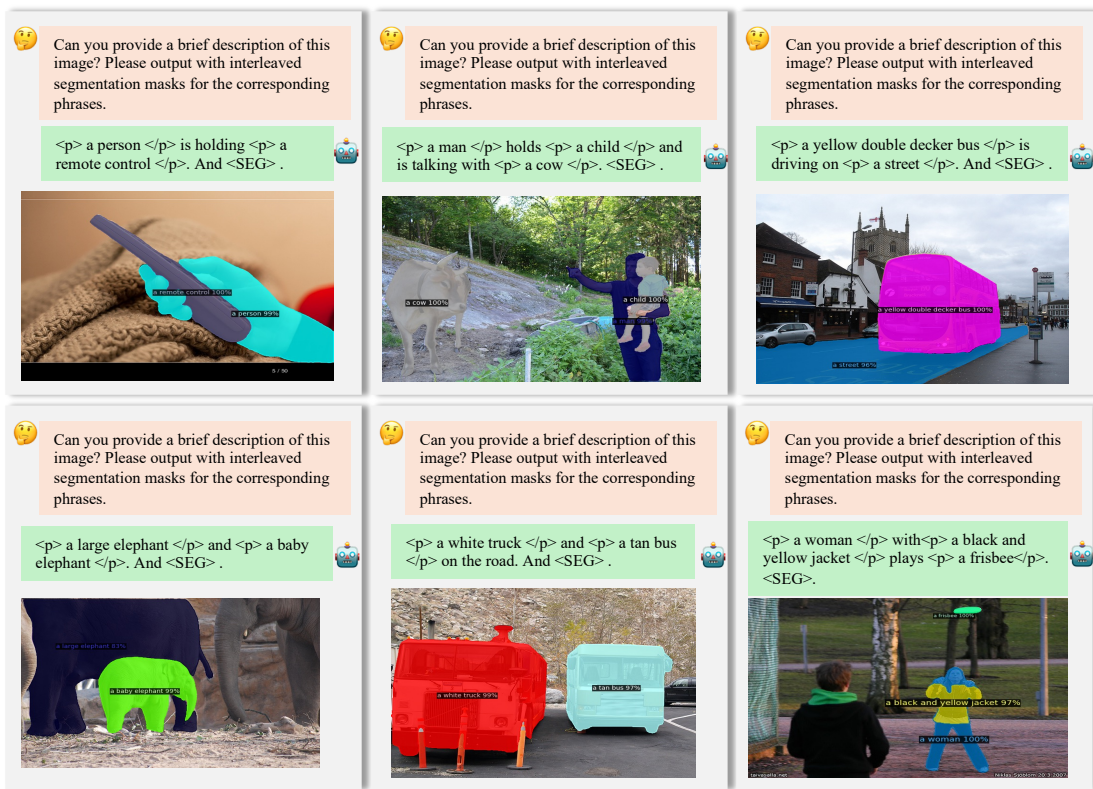


Figure 8: Visualization Results of GCG Segmentation. Visualized images are sampled from the Open-PSG Val set.

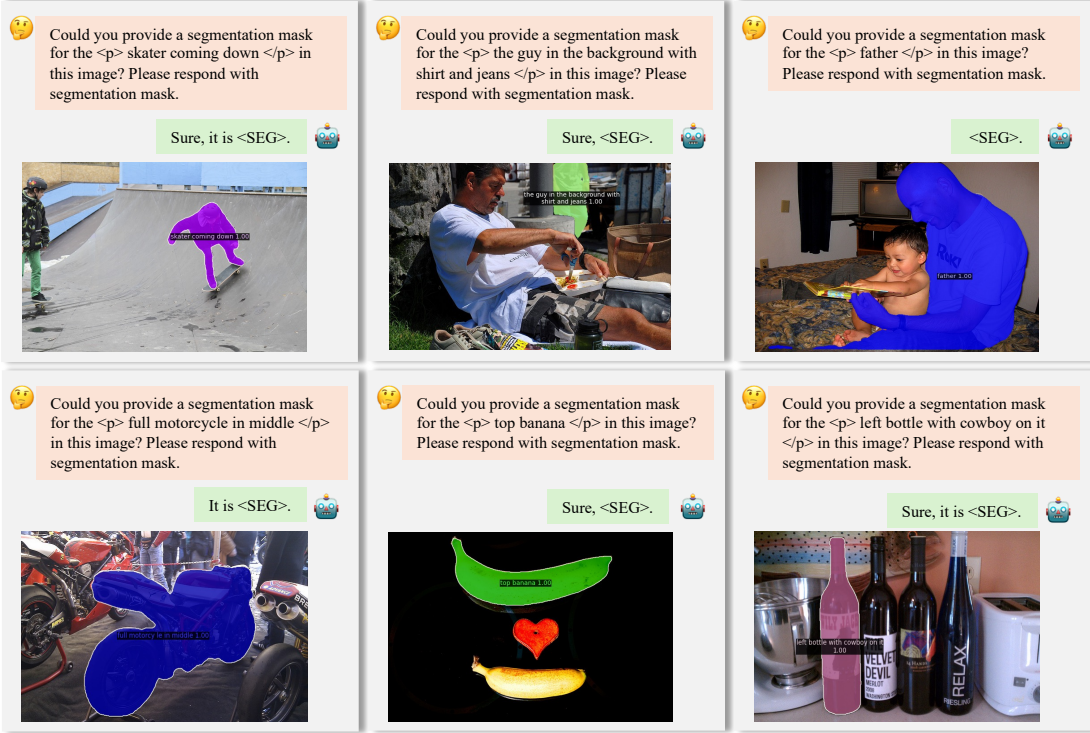


Figure 9: Visualization Results of Referring Segmentation. Visualized images are sampled from the RefCOCO Val set.

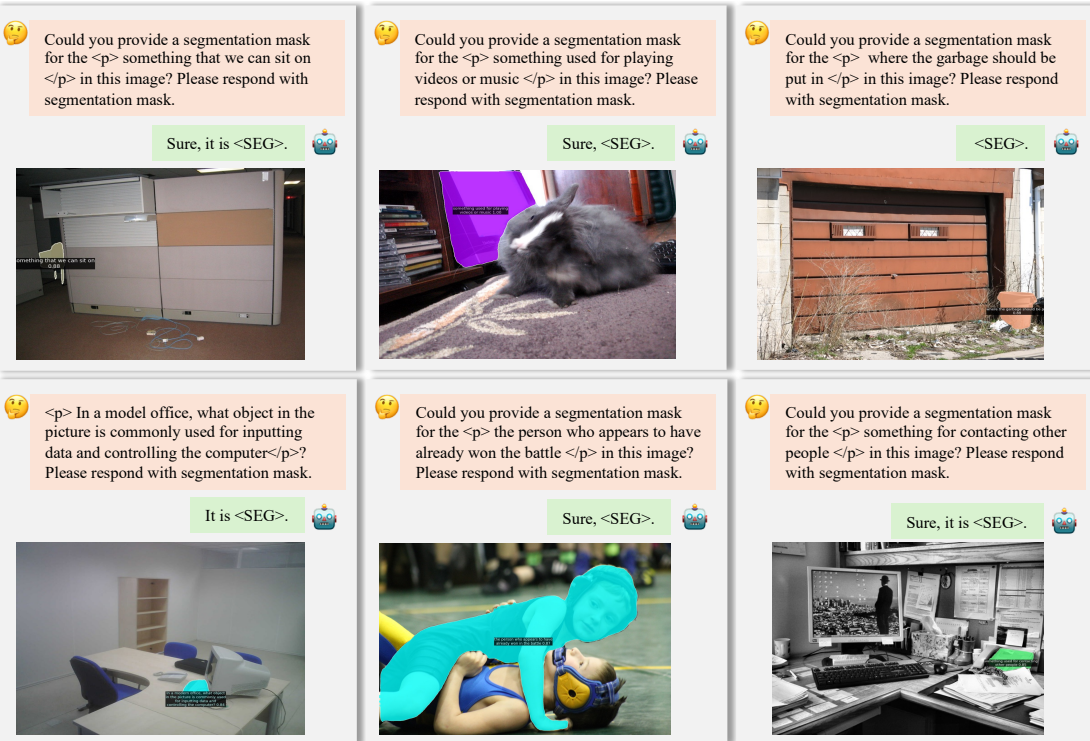


Figure 10: Visualization Results of Reasoning Segmentation. Visualized images are sampled from the reasoning segmentation Val set.



🤔 Can you segment the image based on the following regions: <p><region></p>?
Please respond with segmentation masks.

Sure, it is <SEG>. 🤖



🤔 Can you segment the image based on the following regions: <p><region></p>?
Please respond with segmentation masks.

<SEG>. 🤖

Point Vision Query



🤔 Can you segment the image based on the following regions: <p><region></p>?
Please respond with segmentation masks.

Sure, it is <SEG>. 🤖



🤔 Can you segment the image based on the following regions: <p><region></p>?
Please respond with segmentation masks.

Sure, <SEG>. 🤖

Scribble Vision Query



🤔 Can you segment the image based on the following regions: <p><region></p>?
Please respond with segmentation masks.

Sure, <SEG>. 🤖



🤔 Can you segment the image based on the following regions: <p><region></p>?
Please respond with segmentation masks.

Sure, it is <SEG>. 🤖

Box Vision Query



🤔 Can you segment the image based on the following regions: <p><region></p>?
Please respond with segmentation masks.

<SEG>. 🤖



🤔 Can you segment the image based on the following regions: <p><region></p>?
Please respond with segmentation masks.

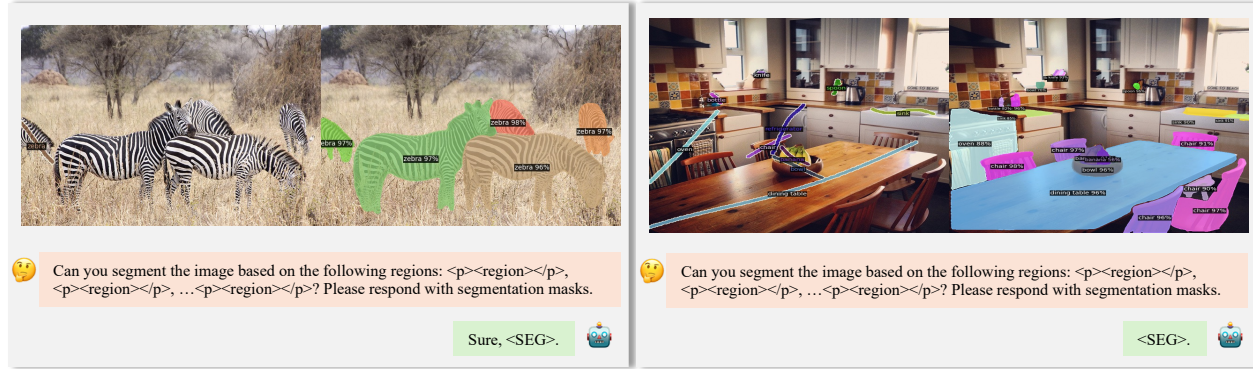
Sure, <SEG>. 🤖

Mask Vision Query

Figure 11: Visualization Results of Interactive Segmentation. Visualized images are sampled from the COCO-Interactive Val set. In each sample, the left image is the original image with the interactive prompts, and the right image is the visualized result of our method. From top to bottom, there are four types of visual interactive prompts: point, scribe, box, and mask. We visualize the category name of the interactive prompt for better visualization.



Point Vision Query



Scribble Vision Query



Box Vision Query



Mask Vision Query

Figure 12: Visualization Results of VGD Segmentation (Single Image). Visualized images are sampled from COCO-VGD Val set. In each sample, the left image is the original image with the visual grounded prompts, and the right image is the visualized result of our method. From top to bottom, there are four types of visual grounded prompts: point, scribble, box, and mask. We visualize the category name of the grounded prompt for better visualization.



🤔 Can you segment the image based on the following regions: <p><region></p>, <p><region></p>, ...<p><region></p>? Please respond with segmentation masks.

<SEG>.

Point Vision Query



🤔 Can you segment the image based on the following regions: <p><region></p>, <p><region></p>, ...<p><region></p>? Please respond with segmentation masks.

Sure, it is <SEG>.



🤔 Can you segment the image based on the following regions: <p><region></p>, <p><region></p>, ...<p><region></p>? Please respond with segmentation masks.

Sure, <SEG>.

Scribble Vision Query



🤔 Can you segment the image based on the following regions: <p><region></p>, <p><region></p>, ...<p><region></p>? Please respond with segmentation masks.

<SEG>.



🤔 Can you segment the image based on the following regions: <p><region></p>, <p><region></p>, ...<p><region></p>? Please respond with segmentation masks.

Sure, it is <SEG>.

Box Vision Query



🤔 Can you segment the image based on the following regions: <p><region></p>, <p><region></p>, ...<p><region></p>? Please respond with segmentation masks.

Sure, <SEG>.



🤔 Can you segment the image based on the following regions: <p><region></p>, <p><region></p>, ...<p><region></p>? Please respond with segmentation masks.

Sure, <SEG>.

Mask Vision Query



🤔 Can you segment the image based on the following regions: <p><region></p>, <p><region></p>, ...<p><region></p>? Please respond with segmentation masks.

<SEG>.



Figure 13: Visualization Results of VGD Segmentation (Cross Image). Visualized images are sampled from the COCO-VGD Val set. In each sample, the left image is a different image with the visual grounded prompts, and the right image is the visualized result of our method. From top to bottom, there are four types of visual grounded prompts: point, scribe, box, and mask. We visualize the category name of the grounded prompt for better visualization.